In this study, we used PDGF-C transgenic (*Pdgf-c* Tg) mice to show that PDGF-C signaling is a possible target of peretinoin in the prevention of hepatic fibrosis, angiogenesis, and the development of HCC.

Materials and Methods

Chemicals

The acyclic retinoid peretinoin (generic name; code, NIK-333) [(2E,4E,6E,10E)-3,7,11,15-tetramethyl-2,4,6,10,14-hexadecapentaenoic acid, C20H30O2, molecular weight 302.46 g/mol] was supplied by Kowa Company.

Animal studies

The generation and characterization of *Pdgf-c Tg* have been described previously (7). Wild-type and *Pdgf-c Tg* mice on a C57BL/6J background were maintained in a pathogen-free animal facility under a standard 12-hour/12-hour light/dark cycle. After weaning at week 4, male mice were randomly divided into the following 3 groups: (1) *Pdgf-c Tg* or wild-type (WT) mice given a basal diet (CRF-1, Charles River Laboratories Japan), (2) *Pdgf-c Tg* or WT mice given a 0.03% peretinoin-containing diet, (3) *Pdgf-c Tg* or WT mice given a 0.06% peretinoin-containing diet. Control mice were normal male homozygotes. At week 20, mice were sacrificed to analyze the progression of hepatic fibrosis ($n = 15$ for each of the 3 groups). At week 48, mice were sacrificed to analyze the development of hepatic tumors ($n = 31$ for the basal diet group, $n = 37$ for the 0.03% peretinoin group, and $n = 17$ for the 0.06% peretinoin group). The incidence of hepatic tumors, maximum tumor size, and liver weight were evaluated. None of the treated WT mice given a diet of 0.03% peretinoin died, but death occurred in 5% of WT mice around after 36 weeks of age receiving a 0.06% peretinoin diet, probably because of its toxicity. In *Pdgf-c Tg* mice, death was observed at similar frequency as WT mice that received 0.06% peretinoin diet.

All animal experiments were carried out in accordance with Guidelines for the Care and Use of Laboratory Animals at the Takara-Machi Campus of Kanazawa University, Japan.

Cell culture

Human HCC cell lines Huh-7, HepG2, and HLE, the mouse fibroblast cell line NIH3T3, human umbilical vein endothelial cells (HUVEC), and human stellate cells Lx-2 (kindly provided by Dr. Scott Friedman, Mount Sinai School of Medicine, New York, NY) were maintained in Dulbecco's Modified Eagle Medium (DMEM; Gibco) supplemented with 10% FBS (Gibco), 1% L-glutamine (Gibco), and 1% penicillin/streptomycin (Gibco) in a humidified atmosphere of 5% CO_2 at 37°C. 1 to 5×10^4 cells were seeded in each well of a 12-well plate the day before serum starvation in serum-free DMEM for 8 hours. The culture medium was then replaced with serum-free medium containing peretinoin. After 24-hour incubation, cells were harvested for analysis.

Isolation and culture of mouse hepatic stellate cells

Hepatic stellate cells (HSC) were isolated from C57BL/6J mice and the effect of recombinant human PDGF-C and peretinoin on HSCs was evaluated *in vitro*. Pronase-collagenase liver digestion was used to isolate HSC from wild-type mice. All experiments were replicated at least twice. Freshly isolated HSCs suspended in culture medium were seeded in uncoated 24-well plates and incubated at 37°C in a humidified atmosphere of 5% CO_2 for 72 hours. Nonadherent cells were removed with a pipette and the culture medium was replaced with medium containing 80 ng/mL recombinant human PDGF-C (Abnova) with or without peretinoin or 9-*cis*-retinoic acid (9cRA; 5 or 10 μmol/L). Cells were harvested for analysis after 24-hour incubation.

Isolation of peripheral blood mononuclear cells

Peripheral blood mononuclear cells were harvested and labeled with FITC-conjugate CD34 (Cell Lab) and R-Phycoerythrin (PE)-conjugated CD31 antibodies (Cell Lab) for 30 minutes at 4°C. After washing with 1 mL PBS, CD31 and CD34 surface expression was measured with a FACSCalibur flow cytometer (BD Biosciences). All flow cytometric data were analyzed using FlowJo software (Tree Star).

Gene expression profiling

Gene expression profiling in mouse liver was evaluated using the GeneChip Mouse Genome 430 2.0 Array (Affymetrix). Liver tissue from WT, *Pdgf-c Tg*, and *Pdgf-c Tg* with 0.06% peretinoin mice all at weeks 20 and 48 was obtained and a total of 34 chip assays were conducted as described previously (17). Expression data have been deposited in the Gene Expression Omnibus (GEO; NCBI Accession; GSE31431).

Pathway analysis was conducted using MetaCore (GeneGo). Functional ontology enrichment analysis was conducted to compare the Gene Ontology (GO) process distribution of differentially expressed genes ($P < 0.01$; refs. 10 and 17). Direct interactions among differentially expressed genes between *Pdgf-c Tg* mice with or without peretinoin administration were examined as reported previously (10). Each connection represents a direct, experimentally confirmed, physical interaction (MetaCore).

Histopathology and immunohistochemical staining

Mouse liver tissues were fixed in 10% formalin and stained with hematoxylin and eosin. The liver neoplasms (HCC and liver cell adenoma) were diagnosed according to previously described criteria (18, 19). Hepatic fibrosis was evaluated by Azan staining. Percentages of fibrous areas were calculated microscopically using an image analysis system (BIOREVO BZ-9000: KEYENCE Japan). Immunohistochemical (IHC) staining was conducted by an immunoperoxidase technique with an Envision kit (DAKO). Primary antibodies used were: rabbit polyclonal PDGFR-α (1:100 dilution), PDGFR-β (1:100 dilution), VEGFR1 (1:100 dilution), desmin (1:100 dilution), β-catenin (1:200 dilution), and mouse monoclonal cyclin D1 (1:400 dilution; all from Cell Signaling Technology); collagen 1 (1:100 dilution), collagen 4 (1:100 dilution), CD31 (1:100 dilution), and CD34 (1:100 dilution; all from Abcam, Cambridge, MA); and Tie-2 (1:80 dilution) and Myc (1:100 dilution; both from Santa Cruz Biotechnology).

Quantitative real-time detection PCR

Total RNA was isolated from frozen liver tissue samples using a GenElute Mammalian Total RNA Miniprep Kit (Sigma-Aldrich) according to the manufacturer's protocol. cDNA was synthesized from 100 ng total RNA using a high-capacity cDNA reverse transcription kit (Applied Biosystems) then mixed with the TaqMan Universal Master Mix (Applied Biosystems) and each TaqMan probe. TaqMan probes used were PDGFR-α/β, VEGFR1/2, α-SMA, collagen 1/4, β-catenin, CyclinD1, and Myc (Applied Biosystems). Relative expression levels were calculated after normalization to glyceraldehyde-3-phosphate dehydrogenase (GAPDH).

Western blotting

Western blotting was conducted as described previously (20). Whole-cell lysates from mouse liver were prepared and lysed by CelLytic MT cell lysis reagent (Sigma-Aldrich) containing Complete Mini EDTA-free Protease Inhibitor cocktail tablets (Roche). Cytoplasmic and nuclear protein extracts were prepared using the NE-PER nuclear extraction reagent kit (Pierce Biotechnology). Primary antibodies used were PDGFR-α (1:1,000 dilution), PDGFR-β (1:1,000 dilution), VEGFR2 (1:1,000 dilution), p44/42 MAPK (1:1,000 dilution), total AKT (1:1,000 dilution), p-p44/42 MAPK (1:1,000 dilution), p-AKT (Ser473; 1:1,000 dilution), p-AKT (Thr308; 1:1,000 dilution), β-catenin (1:2,000 dilution), cyclin D1 (1:400 dilution), and lamin A/C (1:1,000 dilution; all Cell Signaling Technology); α-SMA (1:200 dilution; DAKO); 4-HNE (1:200 dilution; NOF); and GAPDH (1:1,000 dilution) and Myc (1:1,000 dilution; both Santa Cruz).

Statistical analysis

Results are expressed as mean ± SD. Significance was tested by 1-way analysis of variance with Bonferroni's method, and differences were considered statistically significant at $P < 0.05$.

Results

Peretinoin prevented the development of hepatic fibrosis in *Pdgf-c Tg*

To evaluate the HCC chemopreventive effects of peretinoin, we used a mouse model of *Pdgf-c Tg* in which PDGF-C is expressed under the control of the albumin promoter (7). Experimental mice were male mice expressing the PDGF-C transgene (*Pdgf-c Tg*); whereas male mice not expressing the transgene were considered WT. After weaning at week 4, *Pdgf-c Tg* or nontransgenic WT mice were fed a basal diet or a diet containing 0.03% or 0.06% peretinoin. At week 20, mice were sacrificed to analyze the progression of hepatic fibrosis. At week 48, mice were sacrificed to analyze the development of hepatic tumors (Fig. 1A). At week 20, Azan staining showed that predominant pericellular fibrosis had developed in *Pdgf-c Tg* mice (Fig. 1B). Densitometric analysis showed a significant dose-dependent reduction in the size of the fibrotic area in mice that received a diet containing peretinoin at both weeks 20 and 48 (Fig. 1C). Peretinoin therefore efficiently repressed the development of hepatic fibrosis in *Pdgf-c Tg* mice.

The expression of fibrosis-related genes in *Pdgf-c Tg* mice was evaluated by IHC staining, quantitative real-time detection PCR (RTD-PCR), and Western blotting. The expression of PDGFR-α and PDGFR-β, essential receptors for intracellular PDGF-C signaling, was upregulated mainly in the intracellular or portal area in *Pdgf-c Tg* mice livers (Fig. 2), but was significantly repressed by peretinoin after weaning at week 4. Similarly, the expression of collagen 1, collagen 4, and desmin was significantly upregulated in *Pdgf-c Tg* mice, but repressed by peretinoin (Fig. 2 and Supplementary Fig. S1A).

RTD-PCR results confirmed that these genes were substantially upregulated in *Pdgf-c Tg* mice and significantly repressed by both 0.03% and 0.06% peretinoin (Fig. 3A). Western blotting showed that the expression of phosphorylated extracellular signal-regulated kinase (p-ERK) 1/2 and cyclin D1, representative markers of the cell proliferation signaling pathway, was upregulated in *Pdgf-c Tg* mice, and repressed by peretinoin (Fig. 3B). Thus, peretinoin could partially but significantly prevent the development of hepatic fibrosis in *Pdgf-c Tg* mice during the study observation period of 48 weeks.

Peretinoin prevented the development of HCC in *Pdgf-c Tg* mice

At week 48, *Pdgf-c Tg* mice developed hepatic tumors with an incidence of 90% (Fig. 4A). Histologic assessment of these tumors verified that 54% (15/28) were adenomas and 46% (13/28) were HCC (Fig. 4A and C and Supplementary Fig. S2; ref. 21). Peretinoin (0.03%) dose-dependently repressed the incidence of hepatic tumors to 53% (19/36) and to 29% (5/17) at 0.06%. Correlating with tumor incidence, maximum tumor size and liver weight were also significantly repressed by peretinoin (Fig. 4B). Thus, peretinoin repressed the development of hepatic tumors in *Pdgf-c Tg* mice.

Serial gene expression profiling in the liver of *Pdgf-c Tg* mice that developed hepatic fibrosis and tumors

To examine which signaling pathways were altered during the progression of hepatic fibrosis and tumor development, we analyzed gene expression profiling in the liver of *Pdgf-c Tg* mice using Affymetrix gene chips. By filtering criteria for $P < 0.001$ and more than 2-fold differences, 538 genes were selected as differentially expressed. One-way hierarchical clustering analysis of differentially expressed genes is shown in Supplementary Fig. S3.

Of the 3 main clusters, 2 were upregulated (clusters A and B) and 1 was downregulated (cluster C). Cluster A consisted of immune-related [chemokine (C-C motif) receptor (CCR)4, CCR2, toll-like receptor (TLR)3 and TLR4], apoptosis-related [caspase (CASP)1 and CASP9], angiogenesis- and/or growth factor–related (PDGF-C, VEGF-C, osteopontin, HGF), oncogene-related [v-ets erythroblastosis virus E26 oncogene homologue (Ets)1, Ets2, CD44, N-myc downstream-regulated (NDRG)1], and fibrosis-related (tubulin) genes. The expression of cluster A genes was further upregulated in tumors at week

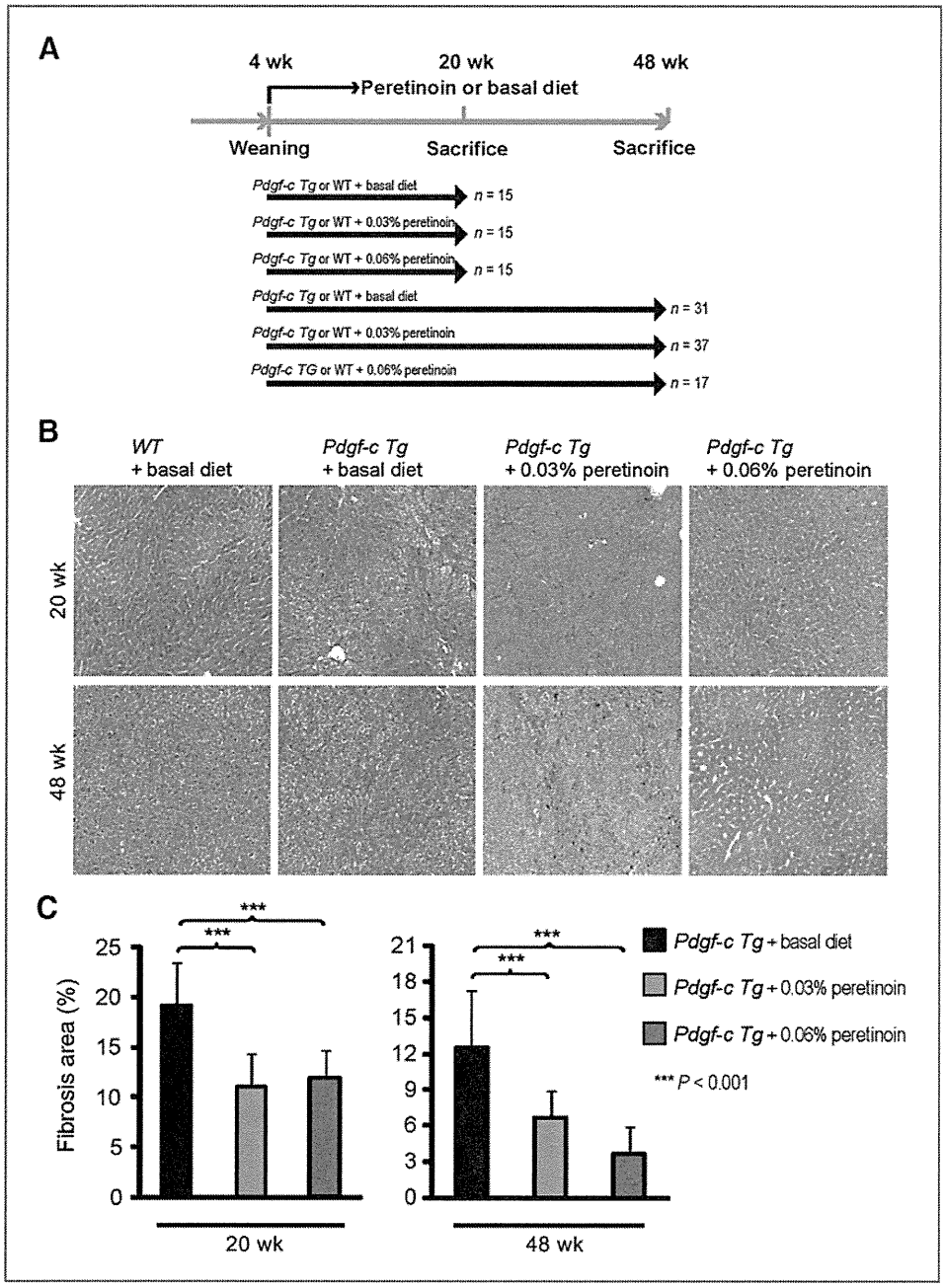

Figure 1. A, feeding schedule of *Pdgf-c Tg* and WT mice. After weaning, male mice were randomly divided into 3 groups: (i) *Pdgf-c Tg* or WT mice receiving basal diet, (ii) *Pdgf-c Tg* or WT mice receiving 0.03% peretinoin-containing diet, and (iii) *Pdgf-c Tg* or WT mice receiving 0.06% peretinoin-containing diet. B, Azan staining of WT or *Pdgf-c Tg* mouse livers fed with different diets at 20 weeks and 48 weeks. C, densitometric analysis of *Pdgf-c Tg* mouse liver fibrotic areas at 20 weeks ($n = 15$) and 48 weeks ($n = 15$).

48. Cluster B consisted mainly of connective tissue- and/or fibrosis-related [vascular cell adhesion molecule (VCAM)1, collagen I, III, IV, V, VI, integrin, decorin, TGF-βRII, PDGFR-α, and PDGFR-β] genes, the expression of which declined slightly at week 48. In contrast, cluster C, containing differentiation and liver function related genes [cytochrome P450, family 2, subfamily c (CYP2C)], were downregulated during the course of hepatic fibrosis and tumor development (Supplementary Fig. S4). Cluster C included xenobiotic- and metabolic process–related genes, which are potential targets of peretinoin. Peretinoin treatment prevented hepatic fibrosis and it preserved liver function. In addition, peretinoin might induce its target genes. Thus, peretinoin reduced the expression of upregulated genes (clusters A and B) and restored the expression of downregulated genes (cluster C) at both weeks 20 and 48 (Supplementary Figs. S3 and S4).

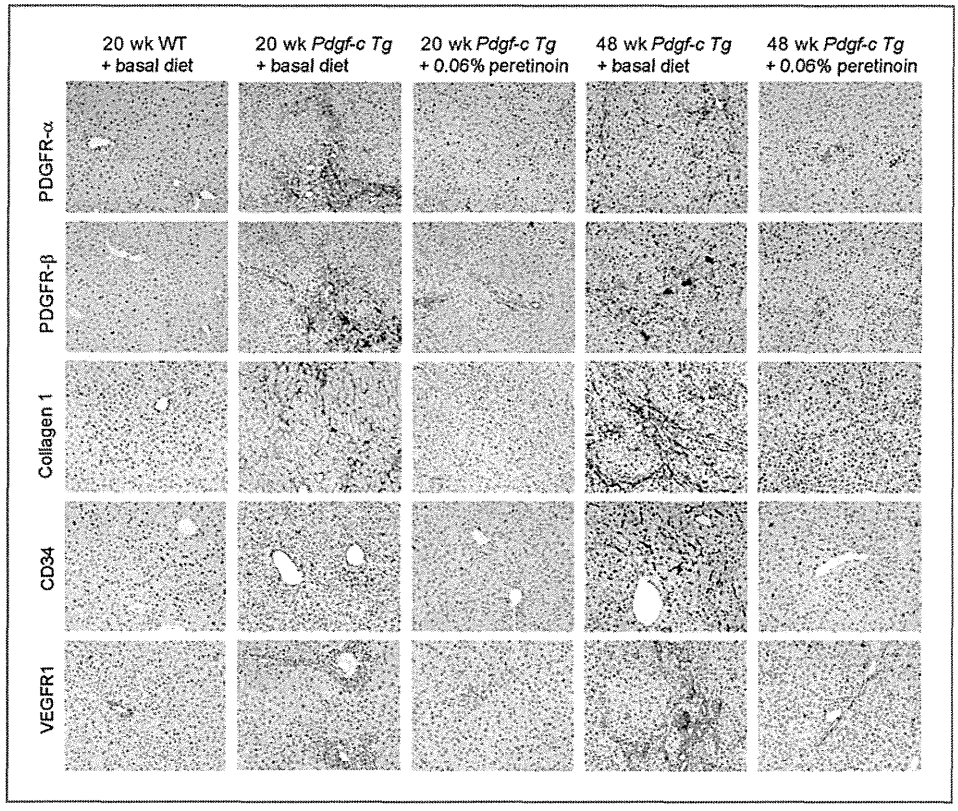

Figure 2. IHC staining of PDGFR-α, PDGFR-β, collagen 1, CD34, and VEGFR1 expression in *Pdgf-c Tg* or WT mouse livers fed a basal diet or 0.06% peretinoin.

To examine the molecular network consisting of differentially expressed genes in *Pdgf-c Tg* mice with or without peretinoin administration, the direct interactions of 513 genes were analyzed by MetaCore (i.e., 413 genes were downregulated and 100 genes were upregulated in *Pdgf-c Tg* mice treated with peretinoin compared with untreated mice; $P < 0.002$). A core gene network consisting of 41 genes was obtained (Supplementary Fig. S5) including interactions between representative growth factors, receptors (PDGFR and TGFβR), and transcriptional factors. Of these genes, the transcriptional factors Sp1 and Ap1 seem to be key regulators in the network (Supplementary Fig. S5).

Peretinoin inhibits PDGFR *in vitro*

Gene expression profiling landscaped the dynamic changes of signaling pathways in *Pdgf-c Tg* mice. To determine the effects of peretinoin *in vitro*, primary HSCs from normal C57BL/6J mice were stimulated by PDGF-C (Fig. 5) to induce the expression of PDGFR-α, PDGFR-β, alpha smooth muscle actin (α-SMA), and collagen 1a2; activated HSCs thus transformed into myofibroblasts (Fig. 5A and B). Peretinoin significantly reduced the expression of these genes and inhibited HSC activation.

We next evaluated the effects of peretinoin on human hepatoma cell lines (Huh-7, HepG2, and HLE), mouse embryonic fibroblast cells (NIH3T3), HUVECs, and Lx-2 (ref. 22; Supplementary Fig. S6A). Experimental conditions were optimized so that more than 90% of cells were variable at 20 μmol/L peretinoin, as determined by an MTS cell proliferation assay (data not shown). Peretinoin dose-dependently inhibited the expression of PDGFR-α and PDGFR-β in Huh-7, HepG2, HLE, NIH3T3, HUVEC, and Lx-2 cells, whereas no obvious expression of PDGFR-α was observed in HepG2 cells and HUVECs (Supplementary Fig. S6A). Peretinoin also inhibited VEGFR2 expression in HUVEC. These results were confirmed by RTD-PCR (data not shown). Correlating with these results, the expression of phosphorylated serine/threonine kinase AKT (p-AKT) and p-ERK1/2, downstream signaling molecules of PDGFR-α, PDGFR-β, and VEGFR2, was also dose-dependently repressed. The expression of collagen 1a2 was significantly repressed by peretinoin in Lx-2, HLE, and Huh-7 cells (Supplementary Fig. S6B). These results suggest that peretinoin may inhibit hepatic fibrosis, angiogenesis, and tumor growth through reduction of the PDGF and VEGF signaling pathway.

We examined the expression of 2 key regulators in peretinoin signaling, Sp1 and Ap1, in Huh-7 cells. Interestingly, the expression of Sp1 was decreased, which correlates with that of PDGFR-α, whereas expression of phosphorylated c-Jun (p-c-Jun) was increased in Huh-7 cells (Supplementary Fig. S6C). Therefore, peretinoin seems to repress the expression of PDGFR, partially through the inhibition of Sp1.

Peretinoin inhibits hepatic angiogenesis in *Pdgf-c Tg* mice

The effect of peretinoin on liver angiogenesis in *Pdgf-c Tg* mice was further analyzed. IHC staining of *Pdgf-c Tg* mouse

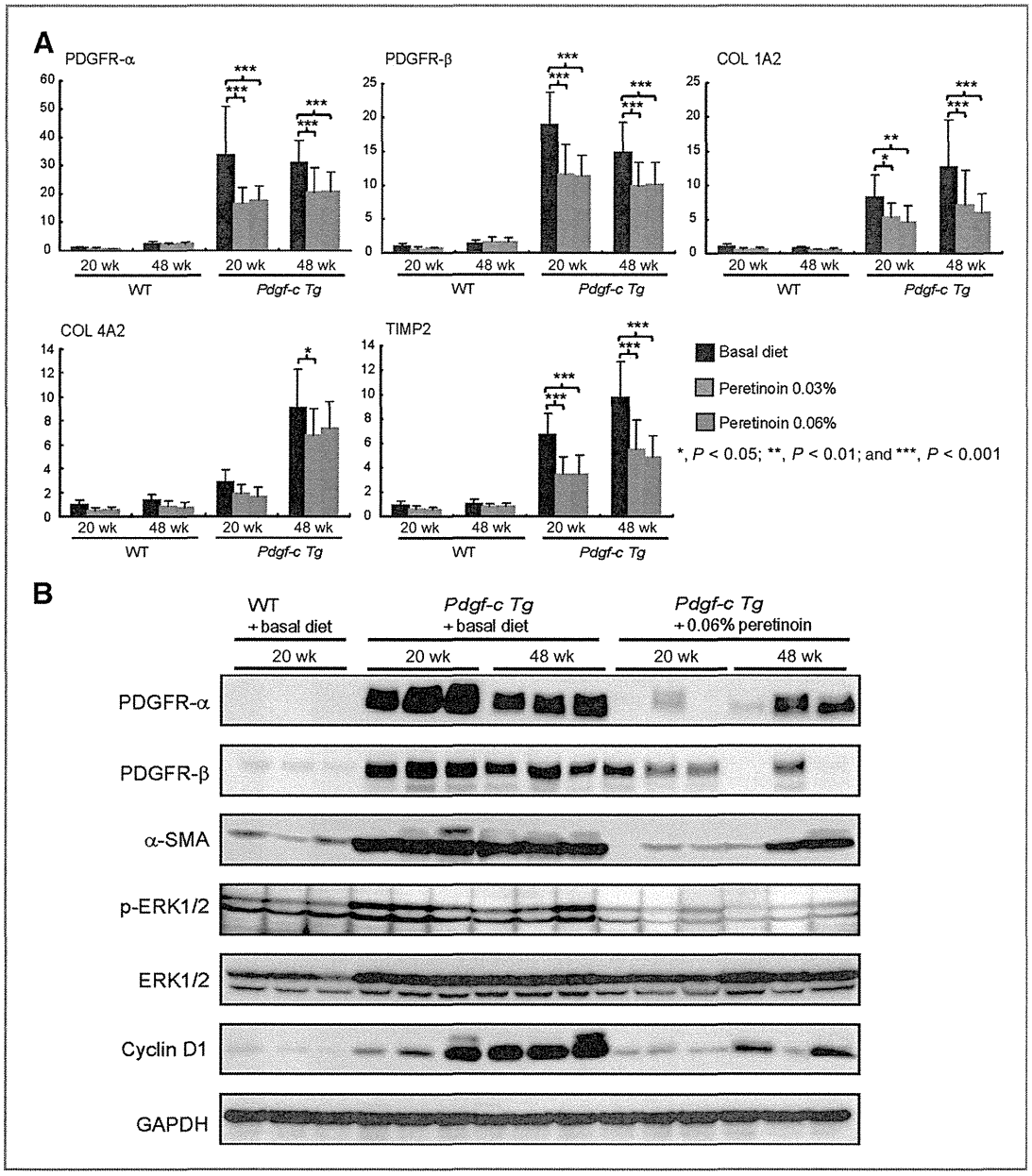

Figure 3. A, RTD-PCR analysis of PDGFR-α, PDGFR-β, collagen (COL) 1a2, collagen 4 a2, and TIMP2 expression in *Pdgf-c Tg* ($n = 5$) or WT mouse livers ($n = 15$). B, Western blotting of PDGFR-α, PDGFR-β, α-SMA, p-ERK, ERK, cyclin D1, and GAPDH expression in PDGF-C Tg or WT mouse livers fed a basal diet or 0.06% peretinoin at 20 or 48 weeks ($n = 3$).

livers at weeks 20 and 48 revealed overexpression of the endothelial markers CD31 and CD34 and the endothelial growth factors VEGFR1 and endothelium-specific receptor tyrosine kinase 2 (Tie2) in the mesenchymal region (Fig. 6 and Supplementary Fig. S1A). This expression was significantly repressed by peretinoin as determined by the densitometric area (Supplemental Fig. S1B). RTD-PCR results revealed significant upregulation of VEGFR1 (Flt-1) in *Pdgf-c Tg* mice compared with WT mice at both weeks 20 and 48, whereas the expression of VEGFR2 (Flk-1) and Tie2 was only upregulated at week 48. The expression of these genes was significantly repressed by peretinoin (Fig. 6A). Western blotting confirmed the upregulation of CD31 and VEGFR1 (Flk-1) at week 48 (Fig. 6B). In addition, p-AKT (Thr 308 and Ser 473) and 4-hydroxy-2-nonenal (4-HNE), an oxidative stress marker, were upregulated in *Pdgf-c Tg* mice and repressed by peretinoin (Fig. 6B).

We also assessed circulating endothelial cells (CEC), a useful biomarker for angiogenesis in the blood, and found that the $CD31^+/CD34^+$ CEC population was significantly upregulated in *Pdgf-c Tg* mice at week 48 but significantly repressed by peretinoin (Fig. 6C and D). Thus, peretinoin

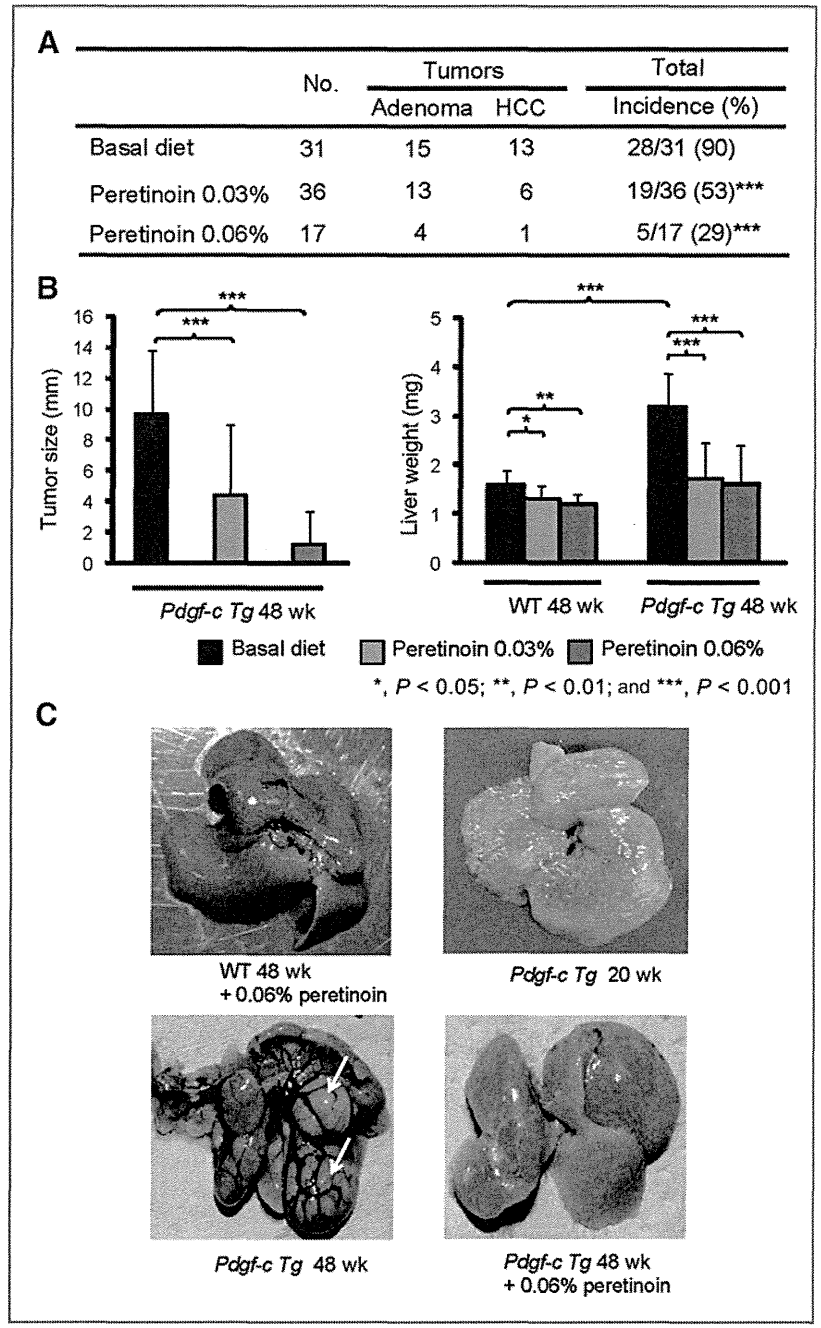

Figure 4. A, incidence of hepatic tumors (adenoma or HCC) in *Pdgf-c Tg* mouse livers fed with different diets. B, tumor sizes and liver weights of *Pdgf-c Tg* and WT mice fed with basal diet ($n = 31$ for *Pdgf-c* Tg, $n = 15$ for WT mice) or 0.03% ($n = 36$ for *Pdgf-c* Tg, $n = 15$ for WT mice) and 0.06% ($n = 17$ for *Pdgf-c* Tg, $n = 15$ for WT mice) peretinoin at 48 weeks. C, macroscopic findings of *Pdgf-c Tg* or WT mouse livers. No obvious change was observed in the liver of WT mice fed with 0.06% peretinoin for 48 weeks (top left). Fibrosis and steatosis were observed in the liver of *Pdgf-c Tg* mice fed a basal diet for 20 weeks (top right). Multiple tumors developed (white arrows) in the liver of *Pdgf-c Tg* mice fed a basal diet for 48 weeks (bottom left). Suppression of tumor development in the liver of *Pdgf-c Tg* mice fed a 0.06% peretinoin diet for 48 weeks (bottom right).

seems to inhibit angiogenesis in the liver of *Pdgf-c Tg* mice, which might prevent the development of hepatic tumors.

Peretinoin inhibits canonical Wnt/β-catenin signaling in *Pdgf-c Tg* mice

The activation of the Wnt/β-catenin signaling pathway is seen in 17% to 40% of patients with primary HCC (23, 24). Moreover, recent reports suggested an interaction between PDGF signaling and Wnt/β-catenin signaling (25–27). We evaluated Wnt/β-catenin signaling in *Pdgf-c Tg* mice and showed by IHC staining that β-catenin was overexpressed in the submembrane at week 48 (Fig. 7A). Peretinoin significantly reduced this expression (Fig. 7A and B), and Western blotting revealed that accumulation of β-catenin in the nuclear fraction of liver tumor tissues was more preferentially repressed by peretinoin than in the cytoplasmic fraction, although expression was repressed in both fractions (Fig. 7C). Wnt ligand (Wnt5a) and frizzled receptor (Fzd1) expression was significantly upregulated in hepatic tumors compared with normal liver (Fig. 7D). These results together suggest that canonical Wnt/β-catenin

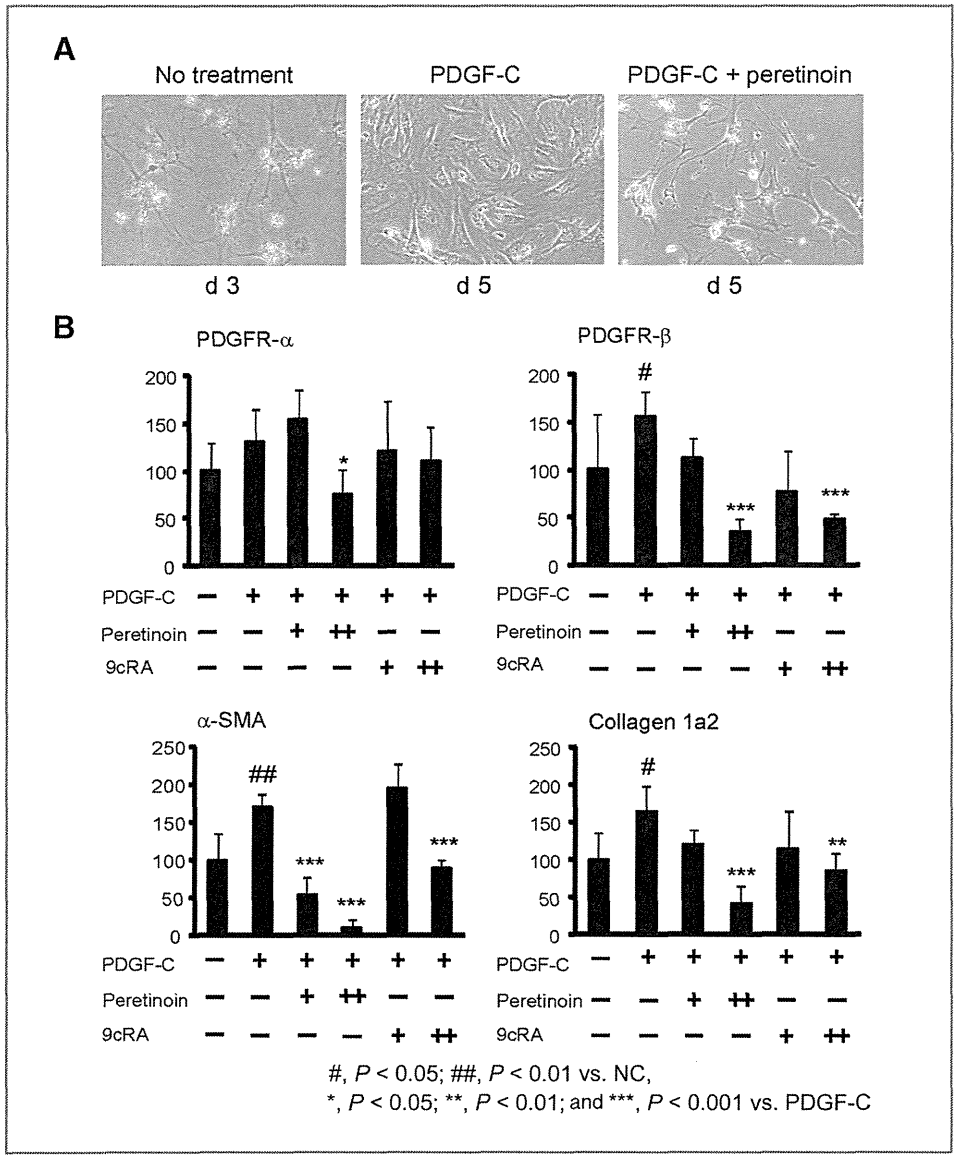

Figure 5. A, microscopic view of freshly isolated primary mouse HSCs after PDGF-C transformation into myofibroblasts (left). Peretinoin inhibited the transformation of HSCs by PDGF-C. B, RTD-PCR analysis of PDGFR-α, PDGFR-β, α-SMA, and collagen 1a2 expression in HSCs treated with or without PDGF-C, peretinoin, and 9cRA ($n = 4$). PDGF-C (+), 80 ng/mL; peretinoin (+), 5 μmol/L; (++), 10 μmol/L; 9cRA (+), 5 μmol/L; (++), 10 μmol/L. NC, no control.

signaling is activated in hepatic tumors and repressed by peretinoin.

Growth factors such as PDGF or HGF potentially activate Wnt/β-catenin signaling (26, 28), which promotes cancer progression and metastasis. We evaluated whether such growth factor signaling could be repressed by peretinoin in hepatic tumors. The expression of c-myc, β-catenin, Tie2, Fit-1, and Flk-1 were significantly upregulated from 1.5- to 4-fold in hepatic tumors compared with normal liver, and this expression was significantly repressed by peretinoin. Similarly, the expression of PDGFR-α, PDGFR-β, collagen 1a2, collagen 4a2, tissue inhibitor of metalloproteinase 2 (TIMP2), and cyclin D1 was substantially upregulated from 5- to 15-fold in hepatic tumors, and significantly repressed by peretinoin (Fig. 7D). Thus, growth factor signaling as well as canonical Wnt/β-catenin signaling in hepatic tumors seems to be repressed by peretinoin. These results explain the inhibitory effect of peretinoin in the development of HCC in *Pdgf-c Tg* mice.

Discussion

HCC often develops in association with liver cirrhosis and its high recurrence rate leads to poor patient prognosis. Indeed, the 10-year recurrence-free survival rate after liver resection for HCC with curative intent was shown to be only 20% (29). Therefore, there is a pressing need to develop effective preventive therapy for HCC recurrence to improve its prognosis.

Peretinoin, a member of the acyclic retinoid family, is expected to be an effective chemopreventive drug for HCC (11, 12, 30) as shown by a previous phase II/III trial in which 600 mg peretinoin per day in the Child-Pugh A subgroup reduced the risk of HCC recurrence or death by 40% [HR = 0.60 (95% CI, 0.40–0.89); ref. 31]. However, further clinical

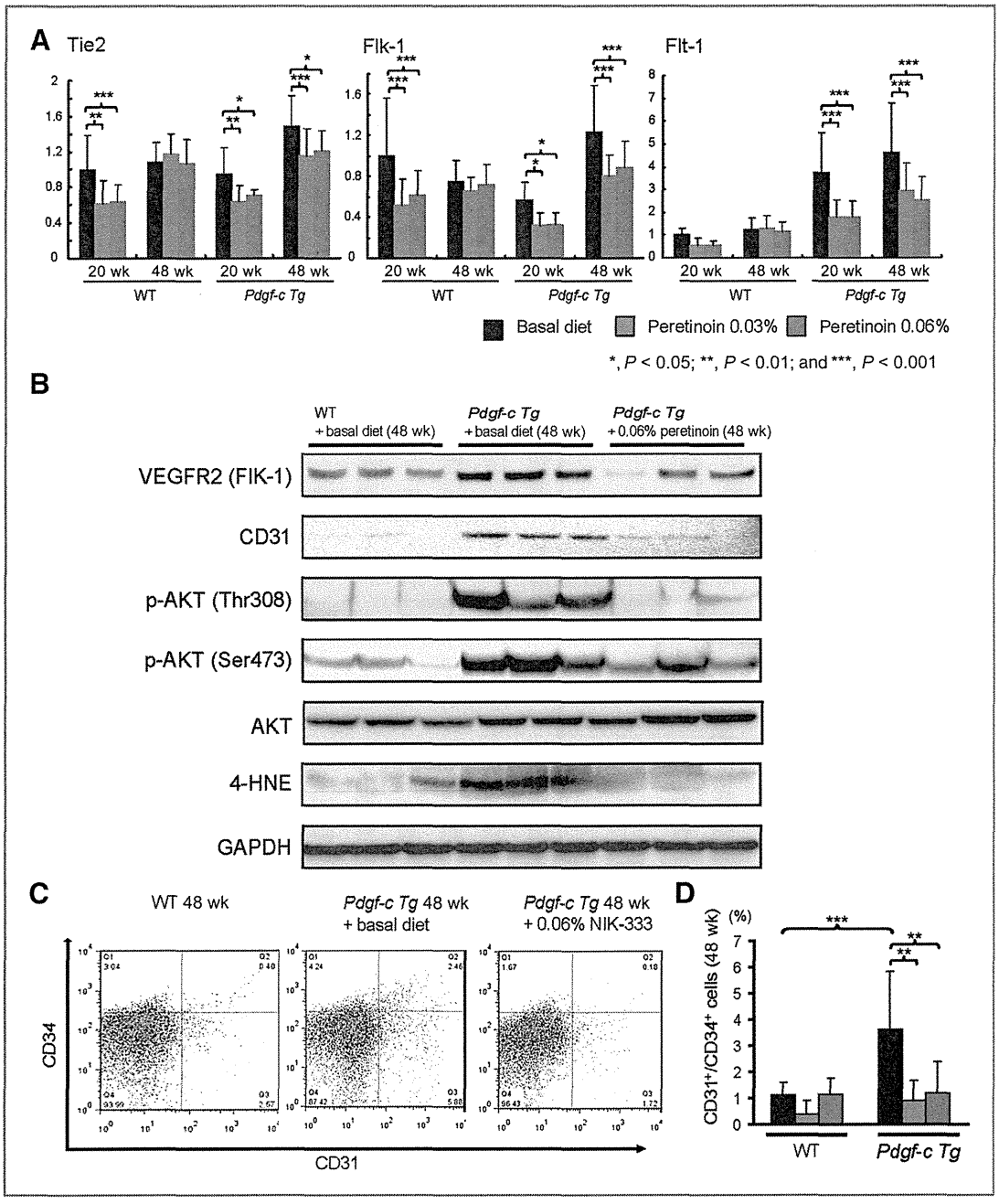

Figure 6. A, RTD-PCR analysis of Tie2, Flk-1, and Flt-1 expression in the liver of *Pdgf-c Tg* and WT mice fed with different diets ($n = 15$). B, Western blotting of Flk-1, CD31, p-AKT (Thr 308, Ser473), AKT, 4-HNE, and GAPDH expression in the liver of *Pdgf-c Tg* or WT mice fed a basal diet or 0.06% peretinoin at 48 weeks ($n = 3$). C, fluorescence-activated cell-sorting analysis of CD31- and CD34-positive CEC in blood of *Pdgf-c Tg* or WT mice fed a basal diet or 0.06% peretinoin at 48 weeks. D, frequency of CD31- and CD34-positive CEC in blood of *Pdgf-c Tg* or WT mice fed a basal diet or 0.06% peretinoin at 48 weeks ($n = 10$).

studies are needed to confirm the clinical efficacy of peretinoin, and a large scale study involving several countries is currently being planned.

During the course of chronic hepatitis, nonparenchymal cells including Kupffer, endothelial and activated stellate cells release a variety of cytokines and growth factors that might accelerate hepatocarcinogenesis. Although peretinoin has been shown to suppress the growth of HCC-derived cells by inducing apoptosis and differentiation (32–35), increasing p21 and reducing cyclin D1 (13), limited data have been published about its effects on hepatic mesenchymal cells such as stellate cells and endothelial cells (14).

In parallel with a phase II/III trial, we conducted a pharmacokinetics study of peretinoin focusing on 12

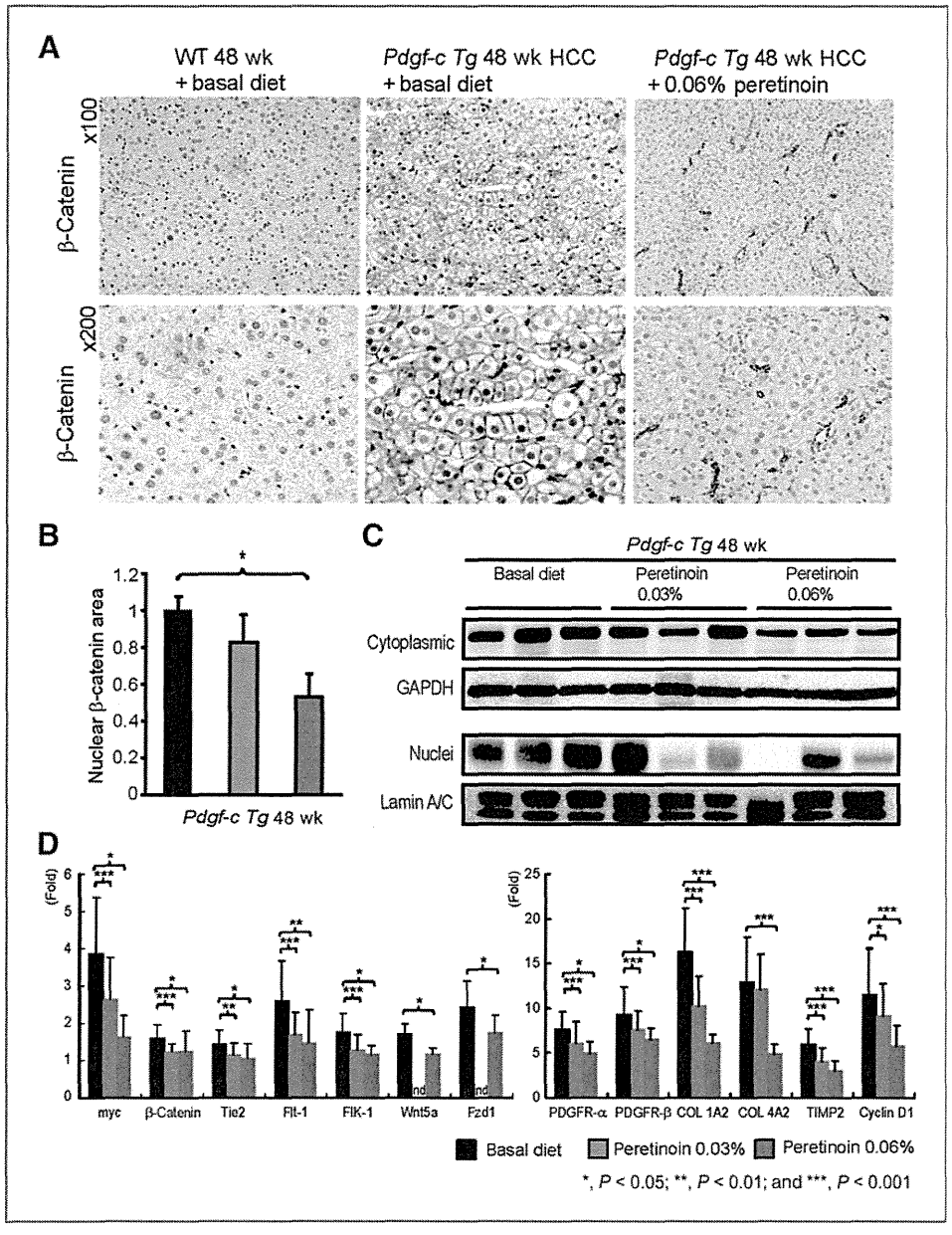

Figure 7. A, IHC staining of β-catenin expression in HCC tissues of *Pdgf-c Tg* mice fed a basal diet or 0.06% peretinoin at 48 weeks. B, densitometric analysis of β-catenin expression in the liver of *Pdgf-c Tg* mice fed with different diets ($n = 15$ for basal diet, $n = 15$ for 0.03% peretinoin, $n = 5$ for 0.06% peretinoin). C, Western blotting of β-catenin expression in cytoplasmic and nuclear fractions of *Pdgf-c Tg* mouse livers fed with different diets. GAPDH was used to standardize cytoplasmic protein and lamin A/C to standardize nuclear protein ($n = 3$). D, RTD-PCR analysis of myc, β-catenin, Tie2, Flt-1, Flk-1, Wnt5a, Fzd1, PDGFR-α, PDGFR-β, collagen (COL) 1a2, collagen 4a2, TIMP2, and cyclin D1 expression in HCC tissues of *Pdgf-c Tg* mice fed with different diets ($n = 15$ for basal diet, $n = 15$ for 0.03% peretinoin, $n = 5$ for 0.06% peretinoin). Relative fold expressions compared with WT mice are shown.

patients with CH-C and HCC to monitor the biological behavior of peretinoin in the liver. Gene expression profiling during peretinoin administration revealed that HCC recurrence within 2 years could be predicted and that PDGF-C expression was one of the strongest predictors. In addition, other genes related to angiogenesis, cancer stem cell and tumor progression were downregulated, whereas expression of genes related to hepatocyte differentiation and tumor suppression was upregulated by peretinoin (data not shown). Moreover, a recent report revealed the emerging significance of PDGF-C–mediated angiogenic and tumorigenic properties (7, 8, 36). In this study, we therefore used the mouse model of *Pdgf-c Tg*, which displays the phenotypes of hepatic fibrosis, steatosis, and HCC development that resemble human HCC arising from chronic hepatitis usually associated with advanced hepatic fibrosis.

We showed that peretinoin effectively inhibits the progression of hepatic fibrosis and tumors in *Pdgf-c Tg* mice (Figs. 1 and 4). Affymetrix gene chips analysis revealed dynamic changes in hepatic gene expression (Supplementary Fig. S3), which were confirmed by IHC staining, RTD-PCR and Western blotting. Pathway analysis of differentially expressed genes suggested that the transcriptional regulators Sp1 and Ap1 are key regulators in the peretinoin inhibition of hepatic fibrosis and tumor development in *Pdgf-c Tg* mice (Supplementary Fig. S5).

We clearly showed that peretinoin inhibited PDGF signaling through the inhibition of PDGFRs (Figs. 2 and 3). In

addition, we showed that PDGFR repression by peretinoin inhibited primary stellate cell activation (Fig. 5). Interestingly, this inhibitory effect was more pronounced than the effects of 9cRA (Fig. 5B). Normal mouse and human hepatocytes neither express PDGF receptors (J.S. Campbell and N. Fausto, unpublished data), nor proliferate in response to treatment with PDGF ligands (7). However, peretinoin inhibited the expression of PDGFRs, collagens, and their downstream signaling molecules in cell lines of hepatoma (Huh-7, HepG2, and HLE), fibroblast (NIH3T3), endothelial cells (HUVEC), and stellate cells (Lx-2; Supplementary Fig. S6). Furthermore, Sp1 but not Ap1, might be involved in the repression of PDGFR-α in Huh-7 cells (Supplementary Fig. 6C). The overexpression of Sp1-activated PDGFR-α promoter activity, whereas siRNA knockdown of Sp1 repressed PDGFR-α promoter activity in Huh-7 cells (data not shown). Therefore, this seems to confirm that Sp1 is involved in the regulation of PDGFR, as reported previously (37, 38), although these findings should be further investigated in different cell lines. A recent report showed the involvement of transglutaminase 2, caspase3, and Sp1 in peretinoin signaling (35).

Peretinoin was shown to inhibit angiogenesis in the liver of *Pdgf-c Tg* mice in this study, as shown by the decreased expression of VEGFR1/2 and Tie 2 (Figs. 2 and 6 and Supplementary Fig. S1). Moreover, peretinoin inhibited the number of $CD31^+$ and $CD34^+$ endothelial cells (CEC) in the blood and liver (Fig. 6C and D), while also inhibiting the expression of EGFR, c-kit, PDGFRs, and VEGFR1/2 in *Pdgf-c Tg* mice (data not shown). We also showed that peretinoin inhibited the expression of multiple growth factors such as HGF, IGF, VEGF, PDGF, and HDGF, which were upregulated from 3- to 10-fold in *Pdgf-c Tg* mice (Supplementary Fig. S3). These activities collectively might contribute to the antitumor effect of peretinoin in *Pdgf-c Tg* mice. The inhibition of both PDGFRs and VEGFR signaling by peretinoin was previously shown to have a significant effect on tumor growth (36), and we confirmed herein that peretinoin inhibited the expression of VEGFR2 in HUVECs (Supplementary Fig. S6; ref. 39). Finally, we showed that peretinoin inhibited canonical Wnt/β-catenin signaling by showing the decreased nuclear accumulation of β-catenin (Fig. 7). These data confirm the previous hypothesis of transrepression of the β-catenin promoter by 9cRA *in vitro* (40).

Although we showed that the PDGF signaling pathway is a target of peretinoin for preventing the development of hepatic fibrosis and tumors in mice, retinoid-inducing genes such as G0S2 (41), TGM2 (35), CEBPA (42), ATF, TP53BP, metallothionein 1H (MT1H), MT2A, and hemopexin (HPX) were upregulated in peretinoin-treated mice (data not shown). These canonical retinoid pathways are likely to participate in preventing disease progression in conjunction with anti-PDGF effects.

The precise mechanism of peretinoin toxicity, in which 5% of mice treated with 0.06% peretinoin died after 24 weeks of treatment, is currently under investigation. These mice showed severe osteopenia and we speculate that the toxicity might be caused by retinoid-induced osteopenia, as observed in a hypervitaminosis A rat model (43). However, the toxicity of prolonged treatment with oral retinoids in humans remains controversial (44) and severe osteopenia has so far only been seen in a rodent model.

In summary, we show that peretinoin effectively inhibits hepatic fibrosis and HCC development in *Pdgf-c Tg* mice. Further studies are needed to elucidate the detailed molecular mechanisms of peretinoin action and the effect of peretinoin on PDGF-C in human HCC. The recently developed multikinase inhibitor Sorafenib (BAY 43-9006, Nexavar) was shown to improve the prognosis of patients with advanced HCC (45). Promisingly, a phase II/III trial of peretinoin showed it to be safe and well tolerated (46). Therefore, combinatorial therapy that incorporates the use of small molecule inhibitors with peretinoin may be beneficial to some patients. The application of peretinoin during pre- or early-fibrosis stage could be beneficial in preventing the progression of fibrosis and subsequent development of HCC in patients with chronic liver disease.

Disclosure of Potential Conflicts of Interest

No potential conflicts of interest were disclosed.

Authors' Contributions

Conception and design: M. Honda, J.S. Campbell, S. Kaneko
Acquisition of data (provided animals, acquired and managed patients, provided facilities, etc.): H. Okada, M. Honda, J.S. Campbell, Y. Sakai, T. Yamashita, Y. Takebuchi, K. Hada, T. Shirasaki, R. Takabatake, M. Nakamura, H. Sunagozaka, N. Fausto
Analysis and interpretation of data (e.g., statistical analysis, biostatistics, computational analysis): J.S. Campbell, T. Yamashita, H. Sunagozaka, S Kaneko
Writing, review, and/or revision of the manuscript: H. OkadaM. Honda, J.S. Campbell, N. Fausto, S. Kaneko
Study supervision: J.S. Campbell, S. Kaneko
Pathologic examination and evaluation: T. Tanaka

Acknowledgments

The authors thank Dr. Scott Friedman, Mount Sinai School of Medicine (New York, NY), for providing Lx-2 cell lines and Nami Nishiyama and Masayo Baba for their excellent technical assistance.

Grant Support

This work was funded by NIH grants CA-23226, CA-174131, and CA-127228 (J.S. Campbell and N. Fausto). This work was also supported in part by a grant-in-aid from the Ministry of Health, Labour and Welfare, and KOWA Co., Ltd., Tokyo, Japan (M. Honda and colleagues).

The costs of publication of this article were defrayed in part by the payment of page charges. This article must therefore be hereby marked *advertisement* in accordance with 18 U.S.C. Section 1734 solely to indicate this fact.

Received January 9, 2012; revised April 27, 2012; accepted May 18, 2012; published OnlineFirst May 31, 2012.

References

1. Befeler AS, Di Bisceglie AM. Hepatocellular carcinoma: diagnosis and treatment. Gastroenterology 2002;122:1609–19.
2. Mohamed AE, Kew MC, Groeneveld HT. Alcohol consumption as a risk factor for hepatocellular carcinoma in urban southern African blacks. Int J Cancer 1992;51:537–41.

3. Tsukuma H, Hiyama T, Tanaka S, Nakao M, Yabuuchi T, Kitamura T, et al. Risk factors for hepatocellular carcinoma among patients with chronic liver disease. N Engl J Med 1993; 328:1797–801.
4. Deugnier YM, Charalambous P, Le Quilleuc D, Turlin B, Searle J, Brissot P, et al. Preneoplastic significance of hepatic iron-free foci in genetic hemochromatosis: a study of 185 patients. Hepatology 1993;18:1363–9.
5. Yeoman AD, Al-Chalabi T, Karani JB, Quaglia A, Devlin J, Mieli-Vergani G, et al. Evaluation of risk factors in the development of hepatocellular carcinoma in autoimmune hepatitis: implications for follow-up and screening. Hepatology 2008;48:863–70.
6. Smedile A, Bugianesi E. Steatosis and hepatocellular carcinoma risk. Eur Rev Med Pharmacol Sci 2005;9:291–3.
7. Campbell JS, Hughes SD, Gilbertson DG, Palmer TE, Holdren MS, Haran AC, et al. Platelet-derived growth factor C induces liver fibrosis, steatosis, and hepatocellular carcinoma. Proc Natl Acad Sci U S A 2005;102:3389–94.
8. Crawford Y, Kasman I, Yu L, Zhong C, Wu X, Modrusan Z, et al. PDGF-C mediates the angiogenic and tumorigenic properties of fibroblasts associated with tumors refractory to anti-VEGF treatment. Cancer Cell 2009;15:21–34.
9. Lau DT, Luxon BA, Xiao SY, Beard MR, Lemon SM. Intrahepatic gene expression profiles and alpha-smooth muscle actin patterns in hepatitis C virus induced fibrosis. Hepatology 2005;42: 273–81.
10. Honda M, Yamashita T, Ueda T, Takatori H, Nishino R, Kaneko S. Different signaling pathways in the livers of patients with chronic hepatitis B or chronic hepatitis C. Hepatology 2006;44: 1122–38.
11. Muto Y, Moriwaki H, Ninomiya M, Adachi S, Saito A, Takasaki KT, et al. Prevention of second primary tumors by an acyclic retinoid, polyprenoic acid, in patients with hepatocellular carcinoma. Hepatoma Prevention Study Group. N Engl J Med 1996;334:1561–7.
12. Muto Y, Moriwaki H, Saito A. Prevention of second primary tumors by an acyclic retinoid in patients with hepatocellular carcinoma. N Engl J Med 1999;340:1046–7.
13. Suzui M, Masuda M, Lim JT, Albanese C, Pestell RG, Weinstein IB. Growth inhibition of human hepatoma cells by acyclic retinoid is associated with induction of p21(CIP1) and inhibition of expression of cyclin D1. Cancer Res 2002;62:3997–4006.
14. Sano T, Kagawa M, Okuno M, Ishibashi N, Hashimoto M, Yamamoto M, et al. Prevention of rat hepatocarcinogenesis by acyclic retinoid is accompanied by reduction in emergence of both TGF-alpha-expressing oval-like cells and activated hepatic stellate cells. Nutr Cancer 2005;51:197–206.
15. Muto Y, Moriwaki H, Omori M. *In vitro* binding affinity of novel synthetic polyprenoids (polyprenoic acids) to cellular retinoid-binding proteins. Gann 1981;72:974–7.
16. Yamada Y, Shidoji Y, Fukutomi Y, Ishikawa T, Kaneko T, Nakagama H, et al. Positive and negative regulations of albumin gene expression by retinoids in human hepatoma cell lines. Mol Carcinog 1994;10:151–8.
17. Honda M, Sakai A, Yamashita T, Nakamoto Y, Mizukoshi E, Sakai Y, et al. Hepatic ISG expression is associated with genetic variation in interleukin 28B and the outcome of IFN therapy for chronic hepatitis C. Gastroenterology 2010;139:499–509.
18. Frith C, Ward J, Turusov V. Pathology of tumors in laboratory animals. Vol. 2. Lyon, France: IARC Scientific Publications; 1994. p. 223–70.
19. Thoolen B, Maronpot RR, Harada T, Nyska A, Rousseaux C, Nolte T, et al. Proliferative and nonproliferative lesions of the rat and mouse hepatobiliary system. Toxicol Pathol 2010;38: 5S–81S.
20. Honda M, Takehana K, Sakai A, Tagata Y, Shirasaki T, Nishitani S, et al. Malnutrition impairs interferon signaling through mTOR and FoxO pathways in patients with chronic hepatitis C. Gastroenterology 2011;141:128–40, 140.e1–2.
21. Frith CH, Ward JM, Turusov VS. Tumours of the liver. IARC Sci Publ 1994;111:223–69.
22. Xu L, Hui AY, Albanis E, Arthur MJ, O'Byrne SM, Blaner WS, et al. Human hepatic stellate cell lines, LX-1 and LX-2: new tools for analysis of hepatic fibrosis. Gut 2005;54:142–51.
23. Nhieu JT, Renard CA, Wei Y, Cherqui D, Zafrani ES, Buendia MA. Nuclear accumulation of mutated beta-catenin in hepatocellular carcinoma is associated with increased cell proliferation. Am J Pathol 1999;155:703–10.
24. Wong CM, Fan ST, Ng IO. beta-Catenin mutation and overexpression in hepatocellular carcinoma: clinicopathologic and prognostic significance. Cancer 2001;92:136–45.
25. van Zijl F, Mair M, Csiszar A, Schneller D, Zulehner G, Huber H, et al. Hepatic tumor-stroma crosstalk guides epithelial to mesenchymal transition at the tumor edge. Oncogene 2009;28: 4022–33.
26. Fischer AN, Fuchs E, Mikula M, Huber H, Beug H, Mikulits W. PDGF essentially links TGF-beta signaling to nuclear beta-catenin accumulation in hepatocellular carcinoma progression. Oncogene 2007;26: 3395–405.
27. Hou X, Kumar A, Lee C, Wang B, Arjunan P, Dong L, et al. PDGF-CC blockade inhibits pathological angiogenesis by acting on multiple cellular and molecular targets. Proc Natl Acad Sci U S A 2010;107: 12216–21.
28. Apte U, Zeng G, Muller P, Tan X, Micsenyi A, Cieply B, et al. Activation of Wnt/beta-catenin pathway during hepatocyte growth factor-induced hepatomegaly in mice. Hepatology 2006;44:992–1002.
29. Eguchi S, Kanematsu T, Arii S, Omata M, Kudo M, Sakamoto M, et al. Recurrence-free survival more than 10 years after liver resection for hepatocellular carcinoma. Br J Surg 2011;98:552–7.
30. Okusaka T, Ueno H, Ikeda M, Morizane C. Phase I and pharmacokinetic clinical trial of oral administration of the acyclic retinoid NIK-333. Hepatol Res 2011;41:542–52.
31. Okusaka T, Makuuchi M, Matsui O, Kumada H, Tanaka K, Kaneko S, et al. Clinical benefit of peretinoin for the suppression of hepatocellular carcinoma (HCC) recurrence in patients with Child-Pugh grade A (CP-A) and small tumor: a subgroup analysis in a phase II/III randomized, placebo-controlled trial. J Clin Oncol 2011;29 Suppl 4s:165.
32. Araki H, Shidoji Y, Yamada Y, Moriwaki H, Muto Y. Retinoid agonist activities of synthetic geranyl geranoic acid derivatives. Biochem Biophys Res Commun 1995;209:66–72.
33. Nakamura N, Shidoji Y, Yamada Y, Hatakeyama H, Moriwaki H, Muto Y. Induction of apoptosis by acyclic retinoid in the human hepatoma-derived cell line, HuH-7. Biochem Biophys Res Commun 1995;207: 382–8.
34. Yasuda I, Shiratori Y, Adachi S, Obora A, Takemura M, Okuno M, et al. Acyclic retinoid induces partial differentiation, down-regulates telomerase reverse transcriptase mRNA expression and telomerase activity, and induces apoptosis in human hepatoma-derived cell lines. J Hepatol 2002;36:660–71.
35. Tatsukawa H, Sano T, Fukaya Y, Ishibashi N, Watanabe M, Okuno M, et al. Dual induction of caspase 3- and transglutaminase-dependent apoptosis by acyclic retinoid in hepatocellular carcinoma cells. Mol Cancer 2011;10:4.
36. Timke C, Zieher H, Roth A, Hauser K, Lipson KE, Weber KJ, et al. Combination of vascular endothelial growth factor receptor/platelet-derived growth factor receptor inhibition markedly improves radiation tumor therapy. Clin Cancer Res 2008;14: 2210–9.
37. Molander C, Hackzell A, Ohta M, Izumi H, Funa K. Sp1 is a key regulator of the PDGF beta-receptor transcription. Mol Biol Rep 2001;28: 223–33.
38. Bonello MR, Khachigian LM. Fibroblast growth factor-2 represses platelet-derived growth factor receptor-alpha (PDGFR-alpha) transcription via ERK1/2-dependent Sp1 phosphorylation and an atypical cis-acting element in the proximal PDGFR-alpha promoter. J Biol Chem 2004;279:2377–82.
39. Komi Y, Sogabe Y, Ishibashi N, Sato Y, Moriwaki H, Shimokado K, et al. Acyclic retinoid inhibits angiogenesis by suppressing the MAPK pathway. Lab Invest 2010;90:52–60.

40. Shah S, Hecht A, Pestell R, Byers SW. Trans-repression of beta-catenin activity by nuclear receptors. J Biol Chem 2003;278: 48137–45.
41. Kitareewan S, Blumen S, Sekula D, Bissonnette RP, Lamph WW, Cui Q, et al. G0S2 is an all-trans-retinoic acid target gene. Int J Oncol 2008;33:397–404.
42. Uray IP, Shen Q, Seo HS, Kim H, Lamph WW, Bissonnette RP, et al. Rexinoid-induced expression of IGFBP-6 requires RARbeta-dependent permissive cooperation of retinoid receptors and AP-1. J Biol Chem 2009;284:345–53.
43. Hough S, Avioli LV, Muir H, Gelderblom D, Jenkins G, Kurasi H, et al. Effects of hypervitaminosis A on the bone and mineral metabolism of the rat. Endocrinology 1988;122: 2933–9.
44. Ribaya-Mercado JD, Blumberg JB. Vitamin A: is it a risk factor for osteoporosis and bone fracture? Nutr Rev 2007;65: 425–38.
45. Llovet JM, Ricci S, Mazzaferro V, Hilgard P, Gane E, Blanc JF, et al. Sorafenib in advanced hepatocellular carcinoma. N Engl J Med 2008;359:378–90.
46. Okita K, Matsui O, Kumada H, Tanaka K, Kaneko S, Moriwaki H, et al. Effect of peretinoin on recurrence of hepatocellular carcinoma (HCC): results of a phase II/III randomized placebo-controlled trial. J Clin Oncol 2010;28 Suppl 15s:4024.

Note: This copy is for your personal non-commercial use only. To order presentation-ready copies for distribution to your colleagues or clients, contact us at *www.rsna.org/rsnarights.*

Hypervascular Hepatocellular Carcinoma: Correlation between Biologic Features and Signal Intensity on Gadoxetic Acid–enhanced MR Images

Azusa Kitao, MD
Osamu Matsui, MD
Norihide Yoneda, MD
Kazuto Kozaka, MD
Satoshi Kobayashi, MD
Wataru Koda, MD
Toshifumi Gabata, MD
Tatsuya Yamashita, MD
Shuichi Kaneko, MD
Yasuni Nakanuma, MD
Ryuichi Kita, MD
Shigeki Arii, MD

Purpose: To analyze the correlation among biologic features, tumor marker production, and signal intensity at gadoxetic acid–enhanced MR imaging in hepatocellular carcinomas (HCCs).

Materials and Methods: Institutional ethics committee approval and informed consent were obtained for this retrospective study. From April 2008 to September 2011, 180 surgically resected HCCs in 180 patients (age, 65.0 years ± 10.3 [range, 34–83 years]; 138 men, 42 women) were classified as either hypointense (n = 158) or hyperintense (n = 22) compared with the signal intensity of the background liver on hepatobiliary phase gadoxetic acid–enhanced MR images. Pathologic features were analyzed and α fetoprotein (AFP) and protein induced by vitamin K absence or antagonist-II (PIVKA-II) production were compared by means of serum analysis and immunohistochemical staining. Recurrence and survival rates were also evaluated. The Mann-Whitney and Pearson correlation tests were used for statistical analysis.

Results: The grade of differentiation was higher (P = .028) and portal vein invasion was less frequent in hyperintense HCCs (13.6%) than in hypointense HCCs (36.7%) (P = .039). The serum levels of AFP, *Lens culinaris* agglutinin reactive fraction of AFP, and PIVKA-II were lower in hyperintense than in hypointense HCCs (P = .003, .004, and .026, respectively). Immunohistochemical AFP and PIVKA-II expression were lower in hyperintense than in hypointense HCCs (both $P < .001$). The recurrence rate was lower in hyperintense than in hypointense HCCs (P = .039).

Conclusion: The results suggest that hyperintense HCCs on gadoxetic acid–enhanced MR images are less aggressive than hypointense HCCs.

©RSNA, 2012

Supplemental material: *http://radiology.rsna.org/lookup/suppl/doi:10.1148/radiol.12120226/-/DC1*

[1] From the Departments of Radiology (A.K., O.M., N.Y., K.K., S. Kobayashi, W.K., T.G.), Gastroenterology (T.Y., S. Kaneko), and Human Pathology (Y.N.), Kanazawa University Graduate School of Medical Science, 13-1 Takaramachi, Kanazawa 920-8640, Japan; Department of Gastroenterology, Osaka Red Cross Hospital, Osaka, Japan (R.K.); and Department of Hepatobiliary-Pancreatic Surgery, Tokyo Medical and Dental University, Tokyo, Japan (S.A.). Received February 9, 2012; revision requested March 27; revision received April 24; accepted May 17; final version accepted June 29. Supported in part by a Grant-in-Aid for Scientific Research (21591549) from the Ministry of Education, Culture, Sports, Science and Technology; and by Health and Labor Sciences Research Grants for "Development of novel molecular markers and imaging modalities for earlier diagnosis of hepatocellular carcinoma." **Address correspondence to** A.K. (e-mail: *kitaoa@staff.kanazawa-u.ac.jp*).

©RSNA, 2012

Hepatocellular carcinoma (HCC) is the most frequent primary malignant hepatic tumor and the third most common cause of cancer death worldwide (1). The accurate detection and characterization of HCC are critical issues in clinical practice for improving the prognosis of patients with HCC.

Gadoxetic acid–enhanced MR imaging is a new imaging modality with high accuracy for diagnosing HCCs (2–4). On images obtained during the hepatobiliary phase of gadoxetic acid–enhanced MR imaging, HCCs commonly show hypointensity when compared with the background liver. However, approximately 6%–15% of hypervascular HCCs demonstrate iso- or hyperintensity, which is uncommon among hepatic malignant tumors (5–8). This hyperintensity was previously shown to be due to overexpression of organic anion transporting polypeptide 8 (OATP8, synonymous with OATP1B3), which might be the uptake transporter of gadoxetic acid in HCCs (5,6). In the normal liver, OATP8 is expressed on the sinusoidal side of the hepatocyte membrane and takes up many intrinsic and extrinsic organic anions from blood into hepatocytes.

On the other hand, Jung et al (9) showed that OATP8 was up-regulated by hepatocyte nuclear factor 1α. These hepatocyte nuclear factors are indispensable transcription factors that relate to primitive embryonal differentiation of hepatocytes and to hepatocarcinogenesis. We suspected that these atypical hypervascular HCCs that show hyperintensity on hepatobiliary phase images (hyperintense HCC) might reflect a distinct subtype of HCC with a particular molecular background and biologic features.

The main tumor marker of HCCs is α-fetoprotein (AFP), especially the *Lens culinaris* agglutinin reactive fraction (L-3). Similarly, the protein induced by vitamin K absence or antagonist-II (PIVKA-II) is a clinically important serum tumor marker. PIVKA-II is an incomplete coagulation factor prothrombin II whose production is related to the absence of vitamin K or the presence of the antagonist of vitamin K, which is the cofactor of γ carboxylase that converts precursor into prothrombin (10). Serum levels of both AFP and PIVKA-II correlate with the histologic degree of malignancy and the prognosis in HCC (11). In addition, there are reports (12,13) showing that AFP expression in HCCs is regulated by several enhancers and suppressors, including the hepatocyte nuclear factor family. Although the molecular basis of PIVKA-II production is not well explained, we speculated that there might be a correlation of the tumor marker production and signal intensity (SI) on hepatobiliary phase images, which would reflect distinct genomic and proteomic expression of HCC.

The purpose of this study was to analyze the correlation among the pathologic and biologic features, tumor marker production, with SI on hepatobiliary phase gadoxetic acid–enhanced MR images of HCCs.

Advances in Knowledge

- Hypervascular hepatocellular carcinomas (HCCs) that hyperintensity relative to the surrounding liver on hepatobiliary phase gadoxetic acid–enhanced MR images demonstrate a significantly higher grade of differentiation ($P = .028$) and rarer portal vein invasion ($P = .039$) than those of hypointense HCCs.
- Hyperintense HCCs on hepatobiliary phase gadoxetic acid–enhanced MR images show significantly lower serum level of α fetoprotein, *Lens culinaris* agglutinin reactive fraction of α fetoprotein, and protein induced by Vitamin K absence or antagonist-II than hypointense HCCs ($P = .003$, $P = .004$, and $P = .026$, respectively).
- Hyperintense HCCs on hepatobiliary phase gadoxetic acid–enhanced MR images similarly show significantly weaker expression of α fetoprotein and protein induced by Vitamin K absence or antagonist-II at immunohistochemical evaluation than did hypointense HCCs (both $P < .001$).
- Hyperintense HCCs on gadoxetic acid–enhanced MR images show a significantly lower recurrence rate than do hypointense HCCs ($P = .039$).

Implication for Patient Care

- Hypervascular HCCs that show hyperintensity on hepatobiliary phase gadoxetic acid–enhanced MR images have biologically less aggressive features than do those that show hypointensity.

Materials and Methods

Patients

This retrospective study received the approval of the institutional ethics committee, and informed consent for using the MR images and resected specimens was obtained from all patients. There were 207 consecutive patients who had 233 HCCs that were surgically resected

Published online
10.1148/radiol.12120226 **Content codes:** GI MR

Radiology 2012; 265:780–789

Abbreviations:
AFP = α-fetoprotein
HCC = hepatocellular carcinoma
L-3 = *Lens culinaris* agglutinin reactive fraction
mAU = milli–arbitrary unit
OATP = organic anion transporting polypeptide
PIVKA-II = protein induced by vitamin K absence or antagonist-II
SI = signal intensity
TR = repetition time

Author contributions:
Guarantors of integrity of entire study, A.K., O.M., K.K., S. Kobayashi, T.G., S. Kaneko, Y.N., S.A.; study concepts/study design or data acquisition or data analysis/interpretation, all authors; manuscript drafting or manuscript revision for important intellectual content, all authors; approval of final version of submitted manuscript, all authors; literature research, A.K., O.M., N.Y., K.K., S. Kobayashi, S. Kaneko, Y.N., S.A.; clinical studies, A.K., O.M., K.K., S. Kobayashi, W.K., T.G., T.Y., S. Kaneko, R.K., S.A.; experimental studies, A.K., N.Y., Y.N., S.A.; statistical analysis, A.K.; and manuscript editing, A.K., O.M., S. Kobayashi, T.G., S. Kaneko, S.A.

Conflicts of interest are listed at the end of this article.

at our institution and six affiliated institutions from April 2008 to September 2011. Patients were excluded if they had more than one HCC (12 patients with 31 nodules), if they had previous treatment (three patients with 10 nodules), if they did not have MR imaging (nine patients with nine nodules) or if their lesions were hypovascular in the arterial phase (three patients with three nodules) (Fig E1 [online]). Average age was 65.0 years ± 10.3 (range, 34–83) (age of men 64.5 years ± 10.5 [range, 34–83 years]; women, 67.4 years ± 9.5 [43–83 years]). Ratio of men to women was 138 (76.7%) to 42 (23.3%). The background liver was normal in 28 patients, whereas 70 patients had chronic hepatitis and 82 had cirrhosis. The origin of liver disease was viral hepatitis type B in 41 patients, type C in 85, types B and C in two, alcoholism in nine, and other origins in 43. Hepatic function was classified as Child-Pugh class A in 169 patients and class B in 11. Average tumor size was 33.8 mm ± 23.4 (range, 7–160 mm).

Gadoxetic Acid–enhanced MR Imaging

Gadoxetic acid–enhanced MR imaging was performed 52.8 days ± 25.3 [range, 3–95 days] before surgical resection for the characterization and pretreatment staging of HCC. MR images were obtained on several MR systems: Signa HDx 1.5 T and 3 T (GE Medical Systems, Milwaukee, Wis), Intera Achieva 1.5 T (Philips Medical Systems, Best, Netherlands), Symphony 1.5 T (Siemens, Erlangen, Germany) and Magnetom Vision 1.5 T (Siemens). MR imaging was performed with fat-suppressed two-dimensional or three-dimensional gradient-echo T1-weighted sequences (repetition time, 3.2–4.0 msec; echo time, 1.6–2.3 msec; flip angle, 10–15 degrees; field of view, 33–42 cm; matrix, 128–192 interpolated to 256–512; section thickness, 4.0–8.0 mm). For dynamic study, a dose of 0.1 mL per kilogram of 0.25 mmol/mL of gadoxetic acid (Primovist, Bayer Schering Pharma, Berlin) was injected intravenously at a flow rate of 1–2.0 mL per second, followed by a 20–40 mL saline flush. To obtain the optimal arterial dominant phase, the following methods were used. In the bolus tracking method, arterial phase timing was determined as the peak time of the abdominal aorta plus 7–15 seconds. In the test injection method (1.5 mL of Primovist + 8 mL saline flush), arterial-phase timing was determined as the peak time of the abdominal aorta plus 10 seconds minus half of imaging time. Portal phase and equilibrium phase images were obtained at 60–90 seconds and 120–180 seconds after injection, respectively. The hepatobiliary phase images were obtained 15–20 minutes after the injection.

Analysis of SI on Gadoxetic Acid–enhanced MR Images

Image analysis was performed by two abdominal imaging radiologists (A.K. and O.M., with 10 and 40 years of experience, respectively) without information on clinical and pathologic results. The SI of the tumor and surrounding background liver was individually measured and then averaged by placing regions of interest during the hepatobiliary phase. The region of interest of the tumor was determined as the maximum oval or round area at the level of the largest diameter of the tumor, avoiding degeneration area and artifact. The average size of the region of interest was 923.6 mm^2 ± 1418.3 (range, 61–6167 mm^2). The average intensity of the entire region of interest was used for analysis. A region of interest of the same size as the tumors was placed on the adjacent liver parenchyma, avoiding the large vessels.

Hypointense HCC was defined as showing lower SI than that of the surrounding liver (tumor SI/background SI < 1.0) (Fig 1a), and hyperintense HCC as showing equal or higher SI (tumor SI/background SI ≥ 1.0) (Fig 2a).

The Enhancement Ratio in the Hepatobiliary Phase

To evaluate the uptake level of gadoxetic acid, we calculated the enhancement ratio of HCCs in the hepatobiliary phase. We could not consistently assess all patients because they were examined with various MR systems and by using somewhat different parameters. As a result, we focused on only 79 HCCs studied at our institution because they were imaged by a variable flip angle method for measuring T1 value. MR images were obtained with either a 1.5-T or 3-T MR system (Signa HDx; GE Medical Systems, Milwaukee, Wis). MR imaging was performed with fat-suppressed three-dimentional spoiled gradient-echo in the steady state T1-weighted sequences (liver acquisition with volume acceleration; generalized encoding matrix; repetition time, 3.2–4.0 msec; echo time, 1.6 msec; flip angle, 6–15 degrees; field of view, 42 × 42 cm; matrix, 192 × 320, interpolated to 512 × 512; section thickness, 4.2 mm; overlap, 2.1 mm). The unenhanced phase was imaged with two different flip angles to calculate the static T1 value. The hepatobiliary phase images were obtained 20 minutes after the injection. The static T1 value before enhancement ($T1_{pre}$) was calculated as follows:

$$\exp(-TR/T1_{pre}) = (SI_A \sin\beta - S_B \sin\alpha)/(SI_A \sin\beta \cos\alpha - SI_B \sin\alpha \cos\beta)$$

where TR is repetition time and SI_A and SI_B represent the signal intensity in flip angle α and β, respectively. The enhanced images were obtained with the same parameters by using flip angle α. Then the T1 value after enhancement ($T1_{post}$) was calculated as follows:

$$\exp(-TR/T1_{post}) = \{SI_{pre}[1-\exp(-TR/T1_{pre})\cos\alpha] + SI_{post}[\exp(-TR/T1_{pre})-1]\} / \{SI_{pre}[1-\exp(-TR/T1_{pre})\cos\alpha] + SI_{post}[\exp(-TR/T1_{pre})-1]\cos\alpha\}$$

The enhancement ratio was shown as (8)

$$(1/T1_{post} - 1/T1_{pre})/(1/T1_{pre})$$

Histologic Diagnosis

Hematoxylin and eosin staining was carried out in tissue sections of all 180

Figure 1

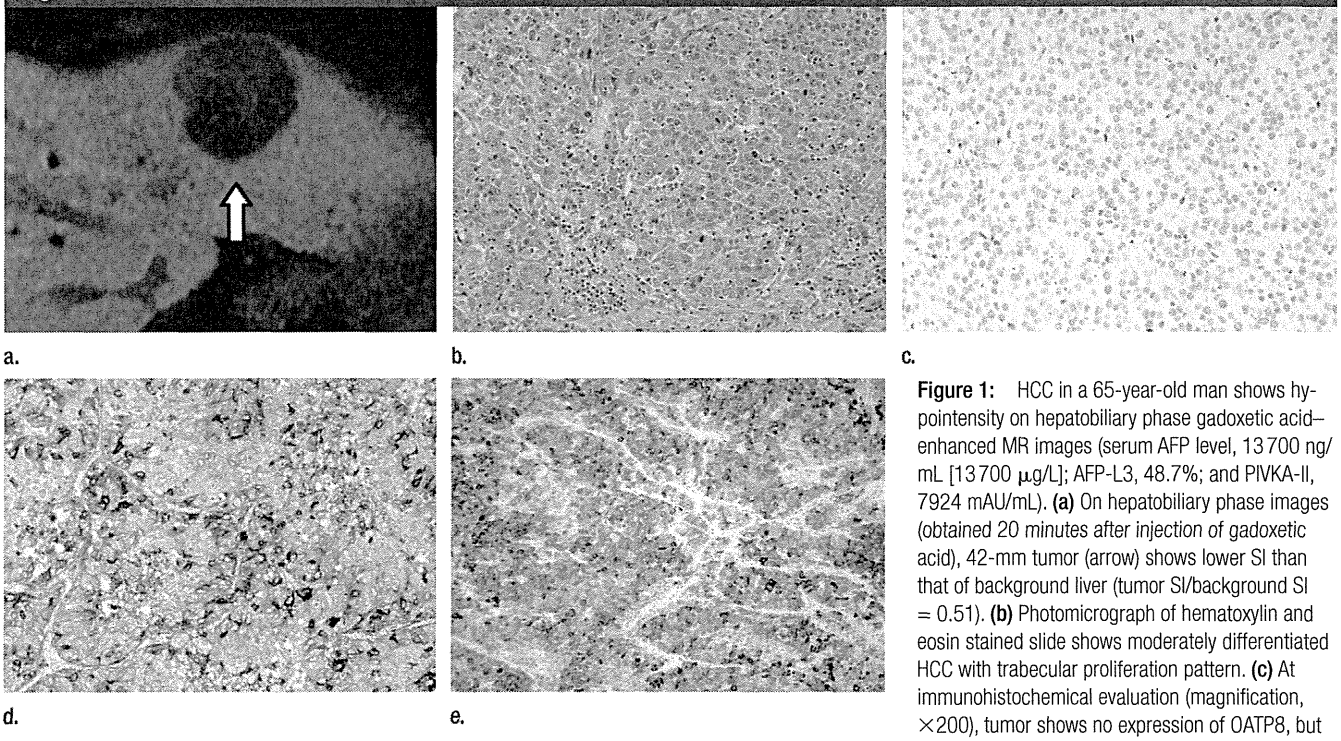

Figure 1: HCC in a 65-year-old man shows hypointensity on hepatobiliary phase gadoxetic acid–enhanced MR images (serum AFP level, 13700 ng/mL [13700 μg/L]; AFP-L3, 48.7%; and PIVKA-II, 7924 mAU/mL). **(a)** On hepatobiliary phase images (obtained 20 minutes after injection of gadoxetic acid), 42-mm tumor (arrow) shows lower SI than that of background liver (tumor SI/background SI = 0.51). **(b)** Photomicrograph of hematoxylin and eosin stained slide shows moderately differentiated HCC with trabecular proliferation pattern. **(c)** At immunohistochemical evaluation (magnification, ×200), tumor shows no expression of OATP8, but **(d)** intense expression of both AFP (brown color) and **(e)** PIVKA-II (brown color).

liver specimens. HCCs were diagnosed by consensus of two liver pathologists (S.K and Y.N. with 10 and 38 years of experience, respectively), according to the classification proposed by the International Working Party (14) and the World Health Organization classification (15). We compared hypointense HCCs and hyperintense HCCs with regard to histologic features such as macroscopic growth patterns (indistinct margin, simple nodular, extranodular growth, and multinodular patterns) (16), differentiation grade (well, moderately, and poorly differentiated), proliferation pattern (trabecular, pseudoglandular, scirrhous, and compact pattern), fibrous capsule invasion, portal vein invasion and hepatic vein invasion.

Measuring Serum Levels of AFP and PIVKA-II

Preoperative patient serum levels were obtained 10.2 days ± 7.3 (range, 0–35 days) before or after MR imaging. Serum AFP levels were measured by using chemiluminescent enzyme immunoassay (Lumipulse presto; Fujirebio, Tokyo, Japan). Serum AFP-L3 levels were measured by means of liquid-phase binding assay-electrokinetic analyte transport assay (LBA AFP-L3; Wako Pure Chemical Industries, Osaka, Japan), and were expressed as the ratio of AFP-L3 to total AFP percentage. Serum PIVKA-II levels were measured by electrochemiluminescence immunoassay (Picolumi PIVKA-II; Eidia, Tokyo, Japan) and were expressed in milli-arbitrary units (mAUs).

Immunohistochemical Analysis of AFP, PIVKA-II, and OATP8

Immunostaining was performed for all HCC specimens by using the primary antibodies human AFP (rabbit polyclonal; DAKO, Glostrup, Denmark), human PIVKA-II (MU-3 mouse monoclonal; Eidia, Tokyo, Japan) and human OATP8 (mouse monoclonal NB100-74482; Novus Biologicals, Littleton, Colo).

Two abdominal imaging radiologists (N.Y. and A.K., with 9 and 10 years of experience, respectively, in radiology and pathologic research) independently and blindly evaluated the intensity of the AFP and PIVKA-II expression on tumor cytoplasm as follows: grade 0, no expression; grade 1, weak expression; grade 2, moderate expression; and grade 3, strong expression. Similarly, they semiquantitatively evaluated the intensity of OATP8 expression on tumor cellular membranes compared with the background hepatocytes as follows: grade 0, no expression; grade 1, decreased expression; grade 2, equivalent expression; and grade 3, increased expression. We analyzed the average grades of the two investigators.

Then, we compared hypointense and hyperintense HCCs for clinical and histologic features and AFP/PIVKA-II expression (serum level and immunohistochemical analysis). To examine whether the AFP and PIVKA level simply correlates with the differentiation grade of HCCs, we performed the same analysis excluding 42 poorly differentiated HCCs. We analyzed the correlation

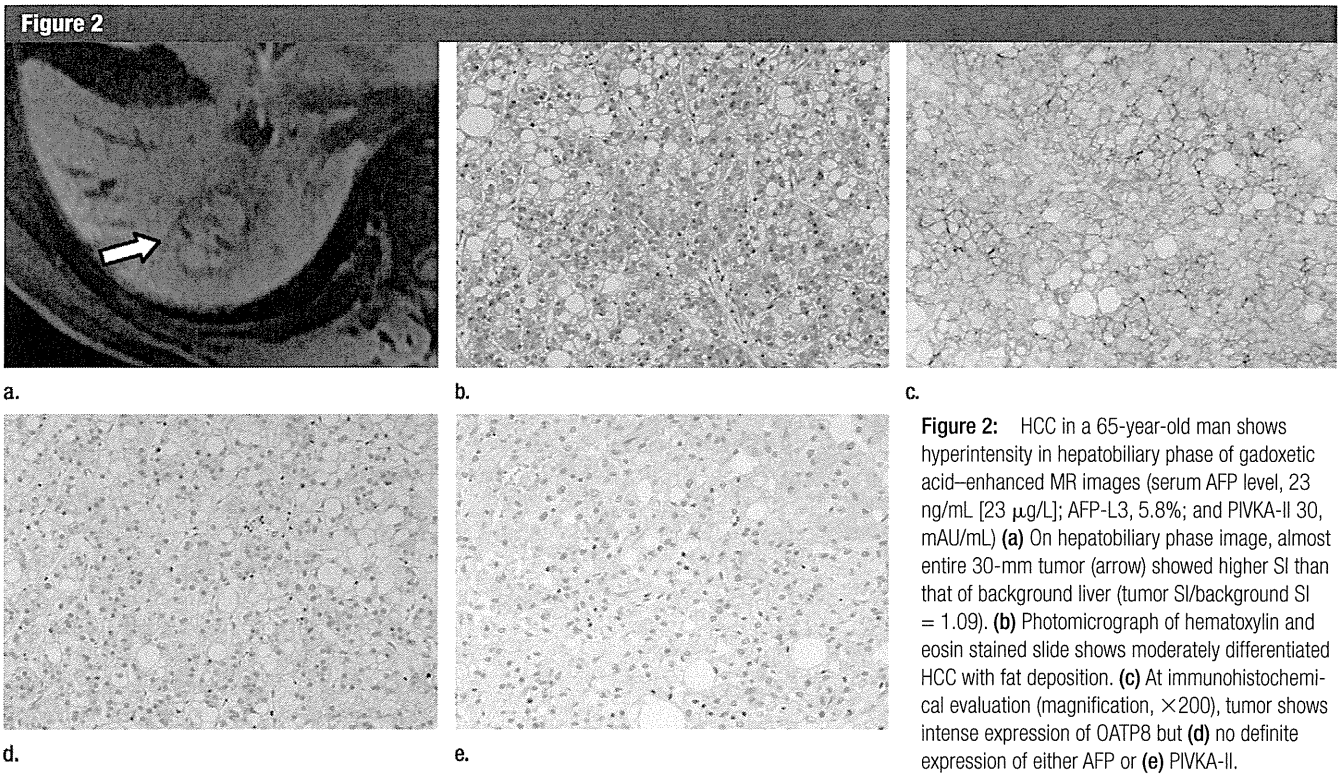

Figure 2: HCC in a 65-year-old man shows hyperintensity in hepatobiliary phase of gadoxetic acid–enhanced MR images (serum AFP level, 23 ng/mL [23 μg/L]; AFP-L3, 5.8%; and PIVKA-II 30, mAU/mL) **(a)** On hepatobiliary phase image, almost entire 30-mm tumor (arrow) showed higher SI than that of background liver (tumor SI/background SI = 1.09). **(b)** Photomicrograph of hematoxylin and eosin stained slide shows moderately differentiated HCC with fat deposition. **(c)** At immunohistochemical evaluation (magnification, ×200), tumor shows intense expression of OATP8 but **(d)** no definite expression of either AFP or **(e)** PIVKA-II.

among the immunohistochemical AFP, PIVKA-II, and OATP8 expression. We also analyzed the correlation among enhancement ratio and serum levels and immunohistochemical AFP and PIVKA-II expression for 79 HCCs.

Recurrence and Survival Rates in Patients with HCC

We compared the two groups for recurrence (including all local recurrence and intrahepatic and extrahepatic metastasis) and survival duration from the operation day. The follow-up length was 727 days ± 365 (range, 22–1293 days). When intrahepatic hypervascular HCCs or obvious extrahepatic metastasis appeared on follow-up dynamic computed tomography or gadoxetic acid–enhanced MR imaging, we considered it to be recurrence.

Statistical Analyses

Statistical significance was evaluated with GraphPad Prism5 (GraphPad Software, San Diego, Calif) and Excel Statistics 2010 (Social Survey Research Information, Tokyo, Japan). We used the Fisher test for the analysis of the clinical and histologic features; Mann-Whitney test for the comparison of serum and immunohistochemical tumor marker levels; Pearson correlation test for the correlations among AFP, PIVKA-II, OATP8 expression and enhancement ratio; and κ test for the evaluation of interobserver variation in the analysis of immunohistochemistry. The κ test score (the level of agreement) was defined as follows: 0.0–0.40, poor; 0.41–0.60, moderate; 0.61–0.80, good to fair; and 0.81–1.0, excellent. Kaplan-Meier analysis with Log-rank test, logistic regression, and Cox regression were performed for the evaluation of clinical outcome and recurrence. A P value less than 0.05 was considered to indicate a statistically significant difference.

Results

Clinical Features of the Two Types of HCC

One hundred and fifty-eight nodules were classified as hypointense HCCs (average tumor SI/background SI, 0.46 ± 0.11; range, 0.24–0.67) and the remaining 22 nodules were classified as hyperintense HCC (average tumor SI/background SI, 1.19 ± 0.22; range, 1.06–1.86). No significant differences were observed in clinical features such as sex, background liver, liver function, or tumor size between the patients with hypointense HCC and hyperintense HCC, but there was a significant difference for age (Table 1). The patients with hyperintense HCCs were significantly older than those with hypointense HCCs (P = .04).

Pathologic Features of the Two Types of HCC

None of the differences noted in the macroscopic growth patterns between the hypointense and hyperintense HCCs were significant (P = .77) (Fig E2a [online]). The hyperintense HCCs showed significantly higher differentiation grade than the hypointense HCCs (P = .028) (Fig E2b [online]). Pseudoglandular pattern was more frequently seen in hyperintense HCCs than in hypointense HCCs (Fig E2c [online]). There was a significant difference in the proliferation

Table 1

Clinical Features of Patients

Clinical Features	Hypointense HCCs	Hyperintense HCCs	*P* Value
No. of tumors	158	22	
Resected tumor size (mm)	33.2 ± 22.9 (7–160)*	37.7 ± 18.9 (10–105)*	.38
Age (y)	64.6 ± 10.3 (34–83)*	69.5 ± 7.8 (52–81)*	.04
Sex			.30
Men	119	3	
Women	39	19	
Background liver tissue			.23
Normal liver	23	5	
Chronic hepatitis	65	5	
Liver cirrhosis	70	12	
Origin of liver disease			.10
Hepatitis B	38	3	
Hepatitis C	74	11	
Hepatitis B and C	2	0	
Alcoholism	6	3	
Other	38	5	
Child Pugh classification			.63
A	149	20	
B	9	2	

Note.—Unless otherwise indicated, data are number of patients.

* Data are means ± standard deviations, with ranges in parentheses.

pattern between the hypointense and hyperintense HCCs ($P < .001$). The hypointense HCCs showed higher positive rates for fibrous capsule invasion and hepatic vein invasion, although the differences did not reach statistical significance ($P = .81$ and .21, respectively). The hyperintense HCCs showed a significantly lower rate of portal vein invasion than that of hypointense HCCs ($P = .039$) (Fig E2e [online]).

Serum Levels of AFP, AFP-L3 Fraction, and PIVKA-II

The serum levels of tumor markers AFP, AFP-L3, and PIVKA-II were significantly lower in the patients with hyperintense HCCs than in those with hypointense HCCs ($P = .003$, .004, and .026) (Figs 3, E3 [online]). To examine whether the AFP and PIVKA levels correlated with the differentiation grade of the HCCs, we performed the same analysis, excluding 42 poorly differentiated HCCs (Fig E4 [online]). Despite excluding poorly differentiated HCCs, the serum levels of these markers were also lower in the patients with hyperintense HCCs than in those with hypointense HCCs ($P = .005$, .019, and .08).

Immunohistochemistry of AFP and PIVKA-II in HCCs

In the semiquantitative analyses of immunohistochemical OATP8, AFP, and PIVKA-II, interobserver agreement of the two readers was good to excellent ($\kappa = 0.82$, 0.78, and 0.81, respectively). In immunohistochemical analysis, OATP8 expression was significantly decreased in hypointense HCCs compared with that in hyperintense HCCs ($P < .001$) (Fig 4a). The AFP expression was significantly higher in hypointense HCCs than that in hyperintense HCCs ($P < .001$) (Fig 4b). There was a significant negative correlation between AFP expression and OATP8 expression ($P = .002$, $R = -0.22$) (Fig E5c [online]). The immunohistochemical PIVKA-II expression was also significantly higher in hypointense HCCs than that in hyperintense HCCs ($P < .001$) (Fig 4c). There was a significant negative correlation between PIVKA-II expression and OATP8 expression ($P < .001$, $R = -0.38$) (Fig E5e [online]). We also performed the same immunohistochemical analysis excluding poorly differentiated HCCs (Fig E6 [online]). The expression of OATP8 was significantly lower, but expression of AFP and PIVKA-II was significantly higher in hypointense HCCs than those in hyperintense HCCs (both $P < .001$). There was still a significant negative correlation between AFP and OATP8 expression ($P = .0017$, $R = -0.27$) and between PIVKA-II and OATP8 expression ($P < .001$, $R = -0.46$).

Relative Enhancement Ratio on Hepatobiliary Phase and AFP or PIVKA-II Production

We analyzed the correlation between relative enhancement ratio and tumor marker expression for 79 HCCs (69 hypointense and 10 hyperintense HCCs). Significant negative correlations were noted among the enhancement ratio and serum AFP ($P = .023$, $R = -0.25$), serum AFP-L3 ($P < .001$, $R = -0.49$) and serum PIVKA-II level ($P = .018$, $R = -0.26$) (Fig E7a, E7b [online]). At immunohistochemical analysis, we also confirmed significant negative correlations among the enhancement ratio and AFP expression ($P = .007$, $R = -0.30$) and PIVKA-II expression ($P = .009$, $R = -0.29$) (Fig E7d, E7e [online]).

Analysis of Prognosis in Patients with HCC

The patients with hyperintense HCCs showed a significantly lower recurrence rate than those with hypointense HCCs ($P = .039$). The patients with hyperintense HCCs tended to show longer survival than those with hypointense HCCs, although without significant difference ($P = .07$) (Fig 5). Clinical features such as age and tumor size did not affect the recurrence and survival curves (Table E1 [online]). The summary of results is shown in Table 2.

Discussion

In our study, hyperintense HCCs in the hepatobiliary phase showed sig

Figure 3

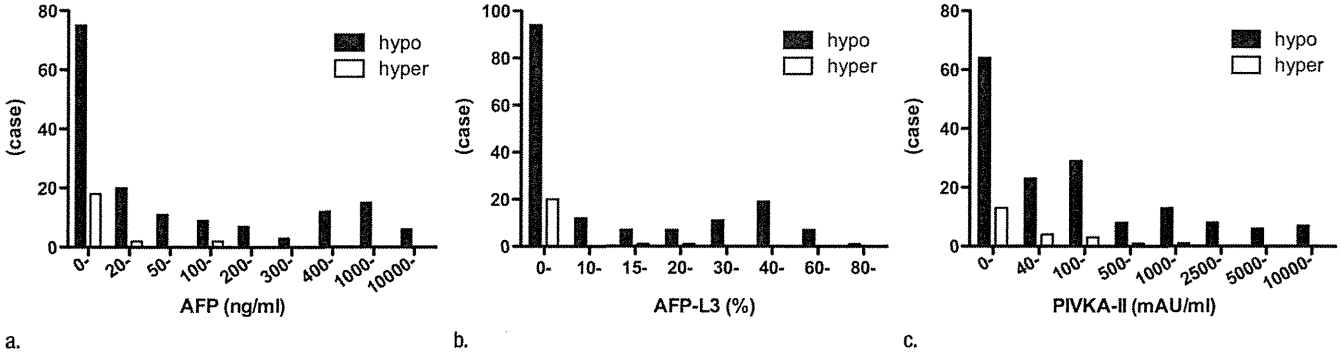

Figure 3: Graphs show serum levels of AFP, AFP-L3, and PIVKA-II. **(a)** Serum level of AFP was in normal range (<20 ng/mL [<20 μg/L]) in 18 of 22 patients (82%) with hyperintense HCCs and in 75 of 158 (47%) of patients with hypointense HCCs. Average serum AFP value was 1202.7 ng/mL ± 4369.9 [1202.7 μg/L ± 4369.9] in patients with hypointense HCCs and 17.9 ng/mL ± 29.0 [17.9 μg/L ± 29.0] in patients with hyperintense HCC, ($P = .003$). **(b)** Serum level of AFP-L3 was in normal range (<10%) in 20 of 22 patients (91%) with hyperintense HCCs, and 94 of 158 (59%) patients with hypointense HCCs. Average serum AFP-L3 fraction value was significantly lower in patients with hyperintense HCC (3.8% ± 7.5) than in those with hypointense HCC (15.9% ± 21.2) ($P = .004$). **(c)** Serum level of PIVKA-II was in normal range (<40 mAU/mL) in 13 of 22 (59%) patients with hyperintense HCCs, and 64 of 158 (40%) patients with hypointense HCCs. The serum level of PIVKA-II was also lower in patients with hyperintense HCCs (190.6 mAU/mL ± 468.6) than those with hypointense HCCs (1697.9 mAU/mL ± 6232.0) ($P = .026$).

Figure 4

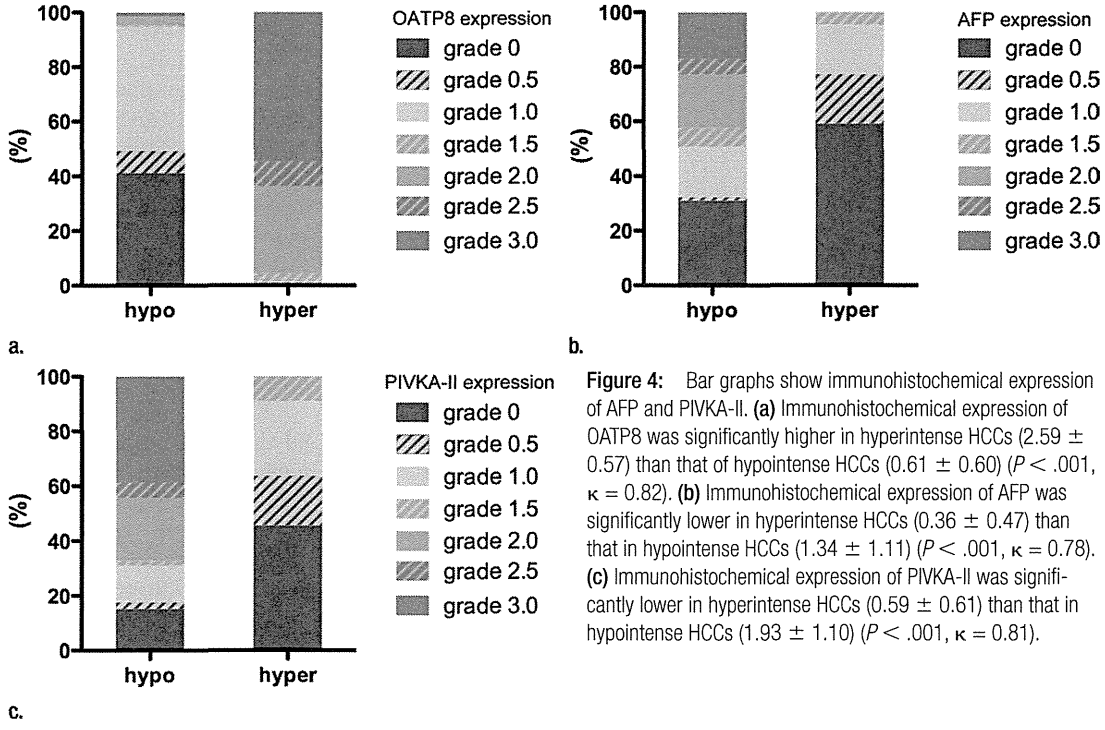

Figure 4: Bar graphs show immunohistochemical expression of AFP and PIVKA-II. **(a)** Immunohistochemical expression of OATP8 was significantly higher in hyperintense HCCs (2.59 ± 0.57) than that of hypointense HCCs (0.61 ± 0.60) ($P < .001$, $\kappa = 0.82$). **(b)** Immunohistochemical expression of AFP was significantly lower in hyperintense HCCs (0.36 ± 0.47) than that in hypointense HCCs (1.34 ± 1.11) ($P < .001$, $\kappa = 0.78$). **(c)** Immunohistochemical expression of PIVKA-II was significantly lower in hyperintense HCCs (0.59 ± 0.61) than that in hypointense HCCs (1.93 ± 1.10) ($P < .001$, $\kappa = 0.81$).

nificantly higher differentiation grades with lower frequency of portal vein invasion than did the hypointense HCCs. Moreover, hyperintense HCCs showed significantly lower expression of AFP and PIVKA-II than did hypointense HCCs. AFP and PIVKA-II levels correlated with the histologic grade of malignancy and poor prognosis (11); however, we demonstrated that the difference in tumor marker production between hypointense HCCs and hyperintense HCCs did not depend on the differentiation grade when poorly differentiated HCCs were excluded

Figure 5

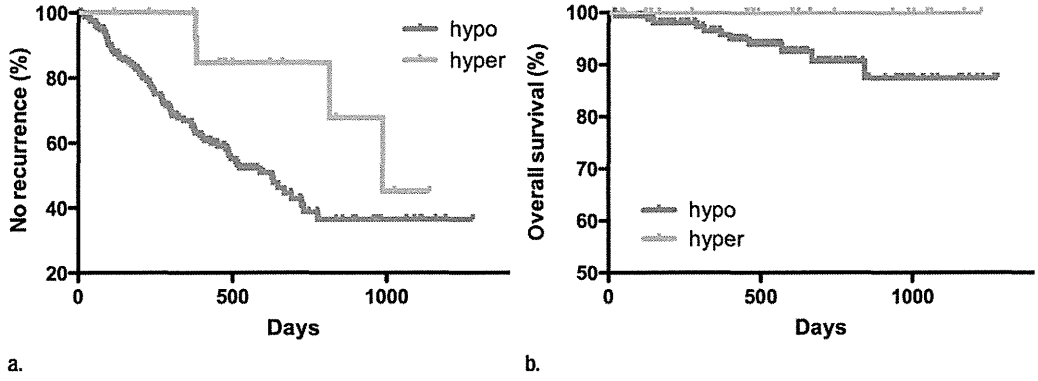

Figure 5: Charts show prognosis of patients with HCC. **(a)** Patients with hyperintense HCCs showed significantly lower recurrence rate (6 of 22, 27.2%) than did those with hypointense HCCs (83 of 158, 52.5%) ($P = .039$). **(b)** Patients with hyperintense HCCs tended to show longer survival (mortality, 0 of 22, 0%) than those with hypointense HCCs (22 of 158, 13.9%). However, there was no significant difference between the two groups ($P = .07$).

Table 2

Summary of Results

Result	Hypointense HCCs ($n = 158$)	Hyperintense HCCs ($n = 22$)	*P* Value
Macro growth pattern			.77
Indistinct margin	6	0	
Simple nodular	102	17	
Extranodular	30	3	
Multinodular	20	2	
Differentiation			.028
Well differentiated	22	4	
Moderately differentiated	94	18	
Poorly differentiated	42	0	
Proliferation pattern			<.001
Trabecular	116	12	
Pseudoglandular	20	10	
Schirrous	9	0	
Compact	13	0	
Fibrous capsule invasion	63 (39.9%)	8 (36.4%)	.810
Portal vein invasion	58 (36.7%)	3 (13.6%)	.039
Hepatic vein invasion	21 (13.3%)	0 (0%)	.210
Serum levels			
AFP (ng/mL)	1202.7 ± 4369.9 (497.4 ± 1899.1*)	17.9 ± 29.0	.003 (.005*)
AFP-L3 (%)	15.9 ± 21.2 (14.5 ± 21.0*)	3.8 ± 7.5	.004 (.019*)
PIVKA-II (mAU/mL)	1697.9 ± 6232.0 (1497.6 ± 7067.9*)	190.6 ± 468.6	.026 (.08*)
Immunohistochemical analysis			
OATP8	0.61 ± 0.60 (0.67 ± 0.63*)	2.59 ± 0.57	<.001 (<.001*)
AFP	1.34 ± 1.11 (1.34 ± 1.10*)	0.36 ± 0.47	<.001 (<.001*)
PIVKA-II	1.93 ± 1.10 (1.87 ± 1.08*)	0.59 ± 0.61	<.001 (<.001*)
Recurrence rate	83 (52.5%)	6 (27.2%)	.039
Survival rate	22 (86.1%)	22 (100%)	.070

* Excluding poorly differentiated HCCs ($n = 42$).

from the analysis. We suspect that the molecular regulatory mechanism of OATP8 expression may have some common channels with those of AFP or PIVKA-II expression.

In addition, hyperintense HCCs on hepatobiliary phase images showed a significantly lower recurrence rate than did hypointense HCCs. The patients with hyperintense HCCs showed longer survival than those with hypointense HCCs, but the difference was not statistically significant. In our study, the follow-up period averaged 727 days, which might not have been sufficient to demonstrate a significant difference.

Several prior reports have suggested that transcription factor hepatocyte nuclear factors control both OATP8 and AFP expression (9,12,13,17). Therefore, we speculated that some correlation between OATP8 and AFP expression through the hepatocyte nuclear factor family might exist. The regulatory mechanism of PIVKA-II and the correlation with OATP8 expression in HCC have not yet been determined. The transcription of the OATP8 gene is also regulated by the nuclear factor (steroid and xenobiotics receptor or pregnane xenobiotics receptor) (18). Vitamin K can be the ligand of these receptors, and it regulates the transcription of target genes (19). If vitamin